Quaternary Science Reviews 363 (2025) 109377

Contents lists available at ScienceDirect

Quaternary Science Reviews

journal homepage: www.elsevier.com/locate/quascirev

Invited Paper

A radiometrically-constrained reference record of Last Interglacial climate and vegetation changes from the Fucino Basin, Central Italy

C.A. Roberts [a,n,*], G. Zanchetta [b,c,d], B. Giaccio [e], S. Nomade [f], G. Mannella [e], L. Sadori [g], R. Drysdale [h], M.A. Maslin [a], P.G. Albert [i,j], C. Smidt [k], V.C. Smith [j], M. Flynn [i], G. Sottili [l], B. Wagner [m], P.C. Tzedakis [a,**]

[a] Environmental Change Research Centre, Department of Geography, University College London, London, United Kingdom
[b] Dipartimento di Scienze della Terra, University of Pisa, Pisa, Italy
[c] Centre for Climatic Change Impact, CIRSEC, University of Pisa, Pisa, Italy
[d] Istituto Nazionale di Geofísica e Vulcanologia (INGV), sez. Pisa, Pisa, Italy
[e] Istituto di Geologia Ambientale e Geoingegneria, Consiglio Nazionale Delle Ricerche, Roma, Italy
[f] Laboratoire des Sciences du Climat et de l'Environnement, LSCE/IPSL, CEA-CNRS-UVSQ and Université Paris-Saclay, Gif-Sur-Yvette, France
[g] Dipartimento di Biologia Ambientale, Università di Roma "LaSapienza", Roma, Italy
[h] School of Geography, Earth and Atmospheric Sciences, University of Melbourne, Australia
[i] Department of Geography, Swansea University, Swansea, United Kingdom
[j] School of Archaeology, University of Oxford, Oxford, United Kingdom
[k] Institute of Geography, University of Bremen, Germany
[l] Department of Earth Sciences, "Sapienza" University of Rome, Rome, Italy
[m] Institute of Geology and Mineralogy, University of Cologne, Cologne, Germany
[n] Department for Environment, Food and Rural Affairs, Seacole Building, Marsham Street, London, United Kingdom

ARTICLE INFO

Handling editor: Antje Voelker

Keywords:
Last interglacial
Pollen
Isotopes
Tephra
$^{40}Ar/^{39}Ar$ dating
Climate variability

ABSTRACT

The Last Interglacial (LIG) was characterised by a global mean temperature ~1 °C warmer than the pre-industrial, a pronounced Arctic warming and an elevated sea level. Exploring the nature of LIG environmental changes in local contexts can improve understanding of regional responses to a warmer background state. However, a lack of high-resolution palaeoclimatic archives underpinned by an independent and robust chronological framework remains a primary limitation in investigating climate variability and relating it to changes in other records. This paper presents a detailed palynological, charcoal and bulk carbonate oxygen isotope record of a thick lacustrine sedimentary sequence retrieved from the Fucino Basin, central Italy, covering the period ~139 to 107 ka at sub-centennial to centennial resolution. A key aspect of the record is its independent chronology based on direct $^{40}Ar/^{39}Ar$ dating and geochemical fingerprinting of several tephra layers. The highly-resolved multiproxy record reveals substantial environmental variability on long- and short-term timescales. The pollen sequence documents a succession of arboreal phases interrupted by centennial-to millennial-scale contractions in temperate vegetation. Comparisons between $\delta^{18}O$ records from the Fucino Basin and a speleothem stack from Corchia Cave (northern Italy) suggest a strong hydrological seasonal contrast during the early LIG, corroborated by increased Mediterranean taxa abundance and elevated fire activity. The early LIG in Italy emerges as a time of high seasonality with arid summers and enhanced winter precipitation driven by strong Northern Hemisphere summer insolation. The detection of high-frequency interglacial climate variability points to an interconnected North Atlantic and Mediterranean climate regime.

1. Introduction

The Last Interglacial (LIG), 129–116 thousand years ago (ka), encompasses the most recent geological interval when climate was largely comparable to modern day (Past Interglacials Working Group of PAGES, 2016). During its early stages, strong eccentricity-precession

* Corresponding author. Environmental Change Research Centre, Department of Geography, University College London, London, United Kingdom.
** Corresponding author.
E-mail addresses: carole.roberts.14@ucl.ac.uk (C.A. Roberts), p.c.tzedakis@ucl.ac.uk (P.C. Tzedakis).

https://doi.org/10.1016/j.quascirev.2025.109377
Received 13 November 2024; Received in revised form 17 April 2025; Accepted 18 April 2025
Available online 26 May 2025

forcing led to intense positive Northern Hemisphere (NH) summer insolation anomalies. This created one of the strongest interglacials of the last 800 ka with 21st June insolation at 65°N reaching a maximum of 538 Wm^{-2} by ~128 ka, exceeding maximum Holocene values (512 Wm^{-2} at 12 ka) (Berger and Loutre, 1991; Past Interglacials Working Group of PAGES, 2016). Climate feedbacks amplified the high-latitude temperature anomalies, as detected in ice-core, marine and terrestrial records (Fairbridge, 1972; Kukla et al., 2002; NGRIP members, 2004; Rohling et al., 2007; Lang and Wolff, 2011; Masson-Delmotte et al., 2011, 2013; NEEM community members, 2013).

In the Arctic, surface air temperatures have been estimated as 3–11 °C higher than pre-industrial values due to polar amplification (CAPE, 2006; Melles et al., 2012), comparable to high-latitude temperature projections for the end of this century (NEEM community members, 2013; Otto-Bliesner et al., 2013, 2021), while estimates for peak LIG global mean surface temperature anomaly range from 0.5 up to 1.5 °C relative to 1850–1900 (Hoffman et al., 2017; Fischer et al., 2018; Gulev et al., 2021).

Although globally reconstructed LIG temperatures are in line with future projections of warming, spatial and temporal temperatures diverge, given the nature of the forcing. While the excess warmth of the LIG resulted from strong NH summer insolation, current and future warming is greenhouse gas-driven (Berger and Loutre, 1991; Ganopolski and Robinson, 2011; Fischer et al., 2018). Though not a perfect analogue to projected future changes, the LIG presents an opportunity to investigate climatic and environmental dynamics under a warm climate state with substantial polar amplification (Capron et al., 2014; Pedersen et al., 2017; Fischer et al., 2018; Shackleton et al., 2020).

Long uninterrupted geological archives with high-resolution environmental records and robust chronological control are essential to investigate LIG climate variability. However, a key limitation remains a lack of independent and robust chronological frameworks in many sedimentary lacustrine successions. To this end, tephrochronology presents a promising solution to developing independent chronologies with recent improvements in the accuracy and precision of distal tephra layer $^{40}Ar/^{39}Ar$ dating and the use of single-crystal laser fusion (Giaccio et al., 2012, 2015, 2017, 2019).

The intense, recurrent explosive activity of the peri-Tyrrhenian volcanoes (Branca et al., 2023) offers an ideal location for the development of detailed tephrochronologies (Giaccio et al., 2017). The Mediterranean region is also a sensitive area for tracking environmental changes as it is strongly influenced by climate patterns across Europe, the North Atlantic, North Africa and Asia (Lionello et al., 2006). Moreover, favourable geological settings and the absence of extensive glacial erosion have allowed the deposition and preservation of long uninterrupted continental sediment records, documenting terrestrial responses over a range of climate background states (Tzedakis et al., 1997). The presence of glacial refugial populations enables the examination of tree-population responses to high-frequency climatic variability with minimal migrational lags (Tzedakis, 1993). Consequently, the Italian, Balkan and Iberian peninsulas have become a key focus for numerous palynological studies investigating vegetation change over glacial-interglacial cycles, for example, Tenaghi Philippon (Wijmstra, 1969; Wijmstra and Smit, 1976; Tzedakis et al., 2006; Milner et al., 2013, 2016; Koutsodendris et al., 2023), Lago Grande di Monticchio (LGdM) (Watts, 1985; Brauer et al., 2007; Allen and Huntley, 2009), Valle di Castiglione (Follieri et al., 1988, 1989), Lake Ioannina (Tzedakis, 1993; Tzedakis et al., 2002, 2003; Roucoux et al., 2008, 2011), Lake Ohrid (Sadori et al., 2016; Sinopoli et al., 2018), Lake Fimon (Pini et al., 2010) and the Padul wetland (Florschütz et al., 1971; Pons and Reille, 1988; Camuera et al., 2018, 2019).

This research aims to assess the nature and extent of environmental changes to long-term and short-term climate variability during the late Penultimate Glacial to early Last Glacial (139–107 ka) at Fucino Basin, central Italy. Earlier studies of a long and continuous lacustrine succession retrieved from the Fucino Basin in the Central Apennines, dated using tephrochronology, demonstrate its potential as a master archive of environmental changes at a centennial-scale over the last 190 ka (Giaccio et al., 2015, 2017; Di Roberto et al., 2018; Mannella et al., 2018, 2019). One of the key objectives, therefore, is to provide a detailed chronology of the late Penultimate Glacial to early Last Glacial based on tephrostratigraphy. A second objective is to generate high-resolution pollen, charcoal and non-pollen palynomorph records of the interval 139-107 ka at Fucino and compare results with previously conducted isotopic analysis undertaken on the same sequence and with other pollen records from southern Europe. Third, to assess the nature and extent of centennial-to millennial-scale climate variability during the late Penultimate Glacial to early Last Glacial in North Atlantic changes (e.g. Tzedakis et al., 2018). A fourth objective is to establish the effect of seasonality by using a complementary speleothem $\delta^{18}O$ record as a proxy of winter recharge to compare to the Fucino $\delta^{18}O$ lacustrine carbonate record, which is mostly an indicator of summer evaporation (Bini et al., 2019; Zanchetta et al., 2022).

2. Study site

2.1. The Fucino Basin

The Fucino Basin (42.00°N, 13.56°E), Central Apennines, is the largest (~300 km^2) of late Neogene-Quaternary intramontane extensional basins occupying the NW-SE Central Apennines Chain (Galadini and Messina, 2004) (Fig. 1). Situated in the Abruzzo region, central Italy, the basin lies at a distance of 80 km from the Tyrrhenian and Adriatic coasts. At an average altitude of 670 m above sea level (m a.s.l.) it is surrounded by some of the highest peaks in the orogenic belt, once occupied by mountain glaciers during glacial intervals (Giraudi, 1989; Giraudi and Giaccio, 2015). The surviving remnants of the "Calderone" glacier still occupy the nearby Gran Sasso peak today (Giraudi, 2002).

The Fucino Basin is a half-graben bounded by an intricate framework of normal and oblique-slip extensional NW-SE-oriented faults, related to Plio-Quaternary extensional tectonics (Cavinato et al., 2002). Representing one of the most tectonically active structures in the Central Apennines, the Fucino Fault System has produced numerous catastrophic earthquakes historically (e.g. Avezzano earthquake, 1915, magnitude = 7.0) (Margottini et al., 1993; Galli et al., 2016). During the Late Pliocene-Early Pleistocene, basin expansion and subsidence generated sediment accommodation space, evolving from sedimentary overfilling and dominant fluvial processes to underfilling and development of a lacustrine environment (Giraudi, 1989; Cavinato et al., 2002). The thickness of the Fucino Basin sedimentary infill increases eastward with the depocenter situated a few km NW of San Benedetto, reaching a maximum thickness of over 1000 m (Giaccio et al., 2019). The Plio-Quaternary alluvial and lacustrine sedimentary succession is relatively unimpacted by sedimentary unconformities or tectonic deformation (Cara et al., 2011). Located downwind of the near peri-Tyrrhenian volcanic centres (100–150 km), the sedimentary sequence contains numerous tephra layers (Giaccio et al., 2015, 2017; Di Roberto et al., 2018; Giaccio et al., 2019; Monaco et al., 2021; Lorenzo Monaco et al., 2022a; Leicher et al., 2023). Several cores have been retrieved from the Fucino Basin and focused investigations have produced a key continental tephrochronological archive and framework for Quaternary palaeoclimatology (Giaccio et al., 2015, 2017; Di Roberto et al., 2018; Mannella et al., 2019; Monaco et al., 2022a; Leicher et al., 2023). This work focuses on core F1-F3 (Fig. 1), recovered from the depo-central area of the basin as part of the "Future project" (Giaccio et al., 2015) Sedimentological analysis reveals no evidence of turbidites over the whole investigated period of 430 ka (Giaccio et al., 2017, 2019).

2.2. Hydrological setting

Fucino Lake was an endorheic basin fed by karstic springs and a network of small streams with the Giovenco River as its main tributary

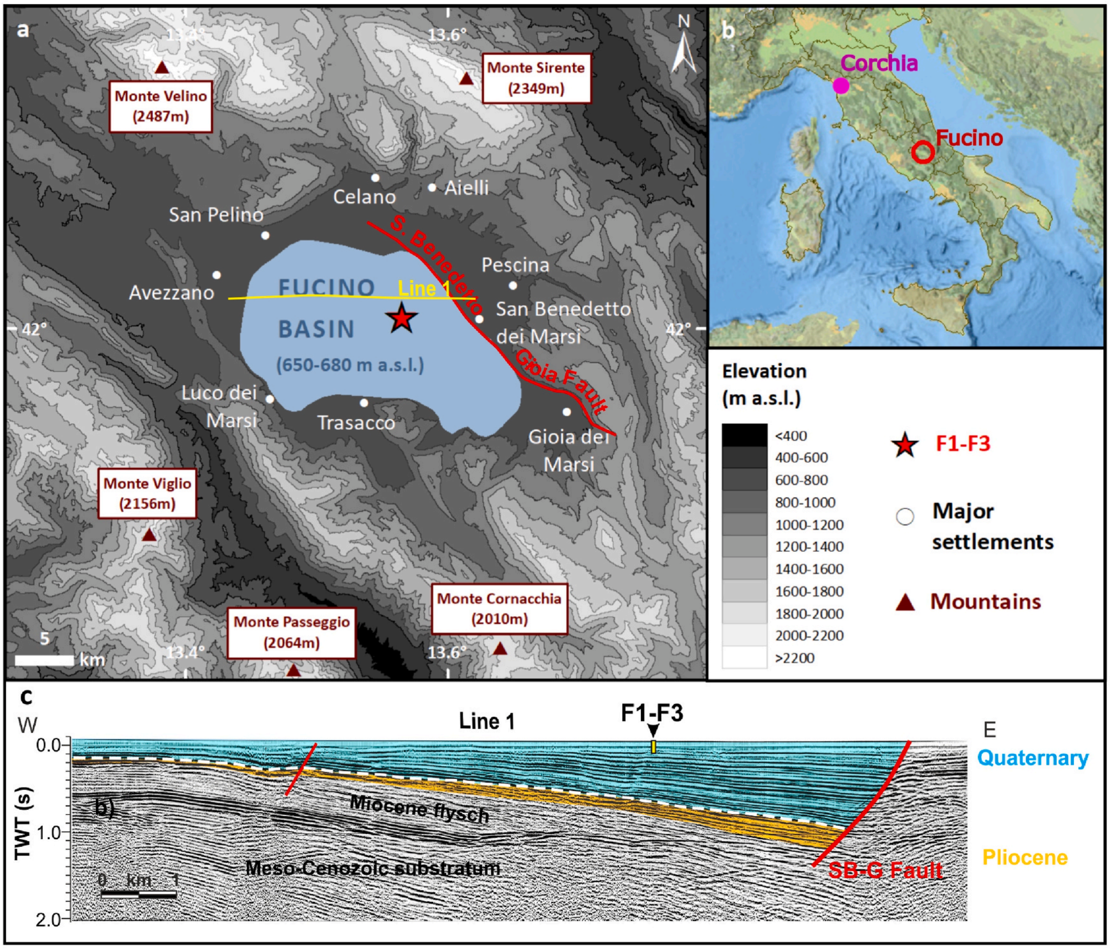

Fig. 1. (a) Elevation of the Fucino Basin (650–680 m a.s.l.) in relation to surrounding peaks (maroon triangles) and major settlements (white dots) (b) Location of the Fucino Basin and Corchia Cave. Red star indicates the location of the F1-F3 core sequence. Blue fill indicates the former extent of the now drained Fucino Lake (c) Seismic line 1 illustrating the internal architecture of the Plio-Quaternary deposits of the Fucino Basin along a W–E transect. The location of the F1-F3 borehole is marked (Giaccio et al., 2024).

draining a 710 km^2 catchment. Located largely along the southern margin, karstic springs currently provide a mean water flow of 6 m^3 s^{-1} to Fucino Basin. Springs are additionally located along the northern shore of the former lake, bordering alluvial fans at the floor of the Sirente-Velino mountain complex (Pacioni, 2008). High recharge rates reaching 800 mm a^{-1} ensure steady discharges from the surrounding streambed and high-discharge springs persisting throughout the dry season (Burri and Petitta, 2004). Situated along the southwestern basin edge, karstic swallow holes once acted as outlets to partially stabilise maximum lake levels (Burri and Petitta, 1998). Following repeated flooding of surrounding settlements, Fucino Lake was first partially drained through an artificial outflow developed by the Romans during the 1st century CE. Before its complete drainage for agriculture in 1875 AD, the lake was the largest in central Italy and overall the country's third-largest lake (Giraudi, 1989, 1998). Large lake-level changes, reconstructed from historical and geological archives, indicate that the lacustrine system was particularly sensitive to hydrological variability (i.e. input/evaporation). This may be a result of a relatively large surface area (140 km^2/volume ratio), with average maximum water depths probably not exceeding 20 m (Giraudi, 1989, 1998).

2.3. Climatic setting

The Apennines represent a natural barrier blocking the eastward movement of Atlantic- and western Mediterranean-sourced moisture, as well as humid air masses from the Adriatic and Tyrrhenian Seas (Drysdale et al., 2004; Lionello et al., 2006). North Atlantic-originating cyclones following a prevailing NW-SE direction along the mid-latitude storm track dominate precipitation in the region, which largely occurs in the winter (Reale and Lionello, 2013). Secondary cyclones form within the Mediterranean basin, in particular the Gulf of Genoa, and are often linked to the movement of major cyclones north of the Mediterranean (Lionello et al., 2006). Summer precipitation is scarcer and mostly in the form of convectional and orographic rainfall with summer droughts occurring alongside the expansion of the Azores high (Xoplaki et al., 2003; Ulbrich et al., 2012).

The Fucino Basin is locally subject to a warm-summer Mediterranean climate with continental characteristics of increased summer humidity and colder winters (Köppen, 1918). Measured climatic data (1991–2021) from Avezzano station (704 m a.s.l.) indicate a maximum between July and August (20–21 °C) and a minimum during January and February (1–2 °C) (Climate Data, 2023) (Fig. 2). As a result of surrounding mountain massifs, the Fucino Basin features moderate annual precipitation (600–750 mm/year), compared to the higher values across much of the Apennines (often >1200 mm/year) (Filibeck et al., 2019).

The nearby L'Aquila station (710 m a.s.l.) recorded local amount-weighted meteoric precipitation $\delta^{18}O$ values of −7.13 ‰ in 2000–2001 (Longinelli and Selmo, 2003). However, the recharge areas of karstic springs feeding the Fucino Basin are located at higher altitude and deliver high spring-season discharge in response to increased snowmelt, effectively lowering $\delta^{18}O$ values to as low as −10 ‰ (Falcone et al., 2008; Petitta et al., 2009; Mariachiara et al., 2014). The isotopic composition is also reduced by the altitude effect, which for $\delta^{18}O$ values is of ca. −0.15 ‰/100 m (Longinelli and Selmo, 2003; Natali et al., 2021).

2.4. Present-day vegetation

From the highest mountains of the Apennine chain (Gran Sasso, Laga, Majella; up to 2912 m a.s.l.) to continental inner basins, the unique bioclimatic and biogeographic characteristics contribute to the high endemism of the Central Apennines (Blasi et al., 2003). Considered as a 'biological crossroads', where various floristic components from distinct biogeographical areas converge, the Abruzzo region records over 3260 plant species out of the 7634 species and subspecies present across the whole of Italy (Conti et al., 2005).

The Fucino Basin is encircled by high-relief terrain, with the present-day flora from the lake plain to the adjacent summits (up to 2912 m.a.s.l) featuring a succession of vegetational belts determined by overriding climate and environmental characteristics (Blasi et al., 2014; Conti and Bartolucci, 2015). Today a natural and semi-natural matrix of forest and natural grasslands (52 %) remains the primary land cover with agricultural areas (46 %) also occupying a substantial extent and artificial surfaces (2 %) comprising the remaining land cover (Blasi et al., 2018).

The sub-Mediterranean climate at lower elevations (below 900 m a.s.l.) supports deciduous thermophile forests of *Quercus pubescens, Quercus cerris, Fraxinus ornus, Ostrya carpinifolia* and *Acer opalus* (Conti and Bartolucci, 2015; Filibeck et al., 2018). Mediterranean formations of *Quercus ilex* woods persist on exposed rocky or steep slopes, while mesophilic woods of *Carpinus betulus* and *Corylus avellane* occur along deeply embanked valleys (De Sillo et al., 2012). Shrubs are characterised by communities of *Rubus ulmifolius, Spartium junceum, Ribes uva-cripa* and several *Rosa* species. Today, much of the deciduous woodland at lower elevations is reduced to a state of coppice interrupted by secondary grassland clearings of the Brometalia order (Conti and Bartolucci, 2015).

Submontane (900–1200 m a.s.l.) and montane belts (1200–1800 m a.s.l.) are dominated by extensive *Fagus sylvatica* forests, which cover 60 % of the National Park of Abruzzo, Lazio and Molise (445 km^2). Secondary Brometalia clearings have fragmented the *Fagus* belt at higher altitudes, consigning much of the beechwoods to a dynamic phase of regeneration. The subalpine (1800–2100 m a.s.l.) and alpine (>2100 m a.s.l.) belts are occupied by primary grasslands, montane heathland *(Juniperus-Vaccinium-Arctostaphylos-Carex),* rocks and screes (Filibeck et al., 2018).

In contrast to the Alps, which experiences a summer maximum in precipitation, the summer rainfall minimum of the Apennines has created a mixture of small, isolated steppic communities together with widespread Mediterranean species in the grassland flora (Blasi et al., 2014; Filibeck et al., 2018, 2019).

3. Materials and methods

3.1. F1-F3 core sediment succession

Cores F1 and F3 (80.27 m and 60.75 m, respectively) were extracted from two boreholes, a few meters away from each other, in the central-eastern area of the Fucino Basin in June 2015 (42.00°N, 13.56°E) (Giaccio et al., 2015) (Fig. 1). The lithology is relatively homogenous and characterised by fine-grained lacustrine deposits, mainly grey calcareous marl and variable in organic matter and clay content (Giaccio et al., 2015; Mannella et al., 2018, 2019). Correlations of individual, overlapping core segments were determined using stratigraphic markers, such as tephra layers and lithological changes, high-resolution line-scan imaging and high-resolution geochemical datasets derived from XRF-scanning as described in Giaccio et al. (2015, 2017) and Mannella et al. (2019). Gas expansion of the recovered sediment core

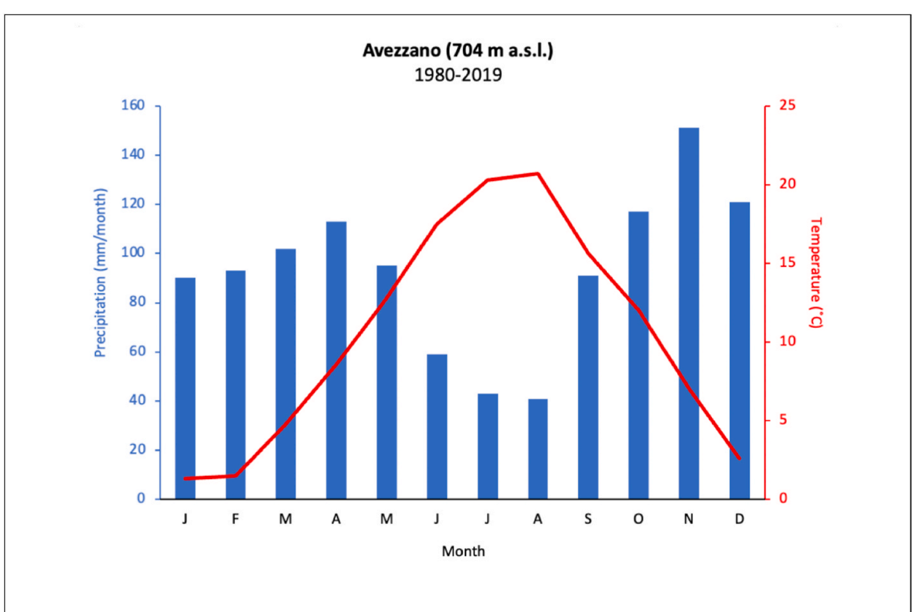

Fig. 2. Average monthly precipitation (mm/month) and temperature (°C) for the period 1991–2021 at Avezzano (704 m a.s.l.) (Climate Data, 2023).

and the systematic selection of more expanded core sections from the parallel cores resulted in a composite section that exceeded the borehole depths (82.70 m) (Giaccio et al., 2015). Disturbed core segments were omitted from the core composite and high-resolution analyses, while tephra layers were removed from the total depth producing a tephra-free core composition in meters below basin floor (m bbf composite) (Mannella et al., 2019).

3.2. Tephrostratigraphy and $^{40}Ar/^{39}Ar$ geochronology

Integrated tephrochronological analyses were carried out on 22 tephra layers of F1-F3 by Giaccio et al. (2015, 2017) and Mannella et al. (2019), and involved Strontium (Sr) and Neodymium (Nd) isotopic studies, and elemental glass composition. Geochemical fingerprinting and correlation of tephra layers combined with direct $^{40}Ar/^{39}Ar$ dating of three tephra layers provide a preliminary chronological framework for the F1-F3 sequence (Fig. 3).

Previous work demonstrated a compositional similarity of the TF-15 and TF-16 layers to the Vico C Ignimbrite and B Ignimbrite, but the collected crystal sizes were too fine (<200 μm) to be dated using the laser single-crystal method. To obtain precise and accurate ages of the Vico B and Vico C ignimbrites, samples for $^{40}Ar/^{39}Ar$ dating were collected in 2018 from proximal sections close to Caparica village, i.e., in the type locality of outcropping of these pyroclastic units (Vico B Ignimbrite; 42°15′11″ N, 12°11′30″ E; Vico C Ignimbrite, 42°15′19″ N, 12°11′02″ E). Ignimbrite B consisted of a single massive unit of more than 10 m thick with homogeneous large dark pumice clasts very rich in large sanidine. Around 5 kg of pumice were collected from the base of this ignimbrite. Ignimbrite C comprises two subunits, a basal ~20 cm-thick Plinian fall (Vico C Plinian) overlain by a plurimetric welded, massive ignimbrite (Vico C Ignimbrite). In order to avoid contamination by older material, a single 30 cm large block of Vico C Plinian and Vico C Ignimbrite pumice comprising sanidine and leucites was collected for dating (see Supplementary Methods for the $^{40}Ar/^{39}Ar$ dating method).

Pilot cryptotephra analysis was conducted on the F1-37 core section, spanning a depth of 58.22–59.72 tephra-free depth below basin floor (bbf) m. Contiguous low-resolution (5 cm) samples were taken throughout this depth interval and samples were subject to the cryptotephra density separation procedures outlined in Blockley et al. (2005), while full details are provided in the Supplementary Methods. A high-powered, polarising optical microscope was used to identify and quantify the volcanic glass shards for each sample. Shard concentrations are quantified as number of shards per gram of dry weight sediment (shards/gram). Where low-resolution F1-37 core section samples revealed cryptotephra (glass) shards, these intervals were re-sampled at high-resolution (1 cm), and processed as above to isolate the peak(s) in glass shard concentrations, and ultimately to resolve the stratigraphic position of the tephra isochron. Major and minor element compositions of individual glass shards were measured using a JEOL-8600 wavelength-dispersive electron microprobe (WDS-EPMA) at the Research Laboratory for Archaeology and the History of Art, University of Oxford. The microprobe was set to an acceleration voltage of 15 kV, a beam current of 6 nA and utilised a 10 μm beam diameter. Further analytical details are found in the Supplementary Methods.

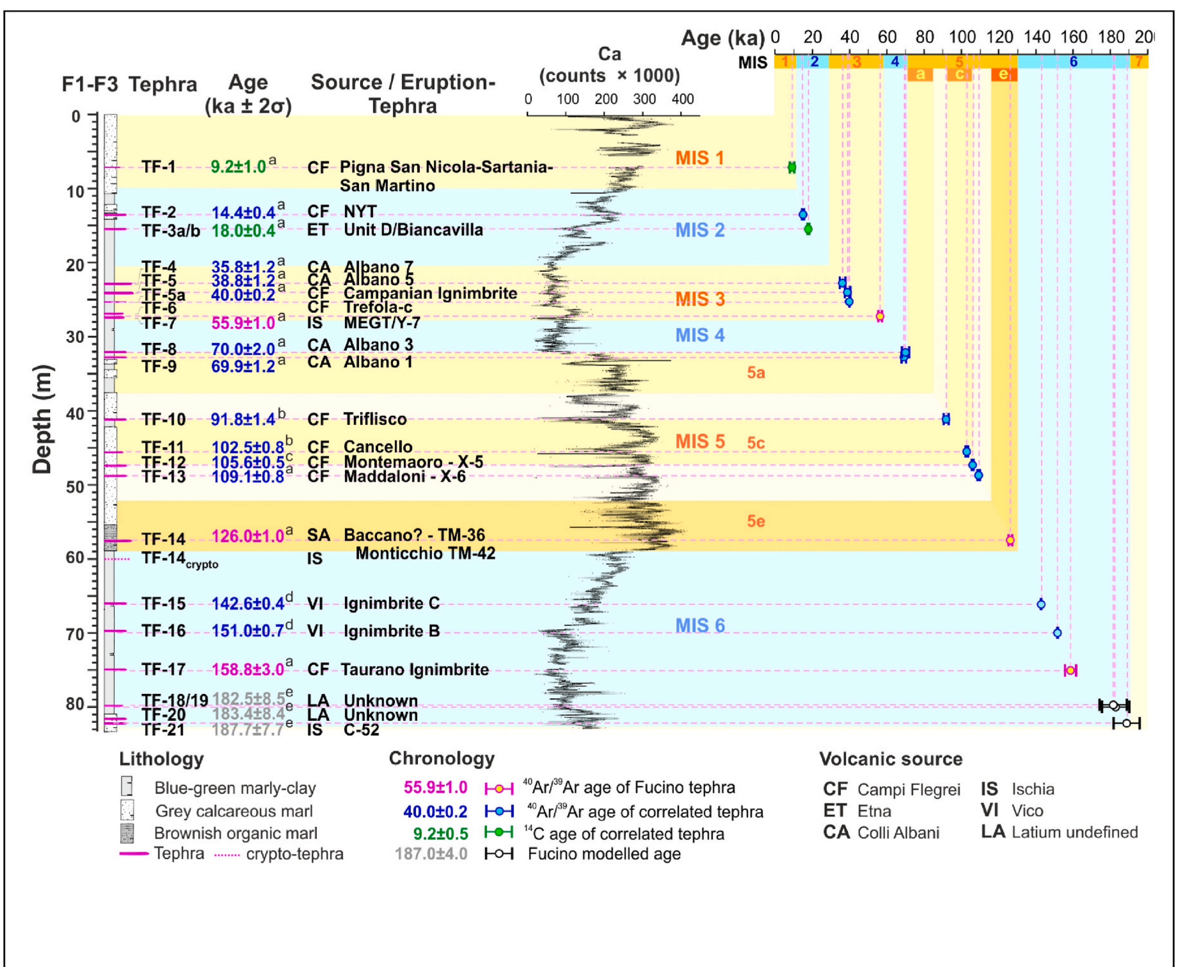

Fig. 3. Litho- and tephrostratigraphy of F1-F3 sequence, along with ages of dated and fingerprinted tephras displayed against XRF Ca counts.

3.3. Age-depth model

The age model applied here is updated from Mannella et al. (2019), incorporating new $^{40}Ar/^{39}Ar$ dates for the Vico B Ignimbrite (TF-16) and C Ignimbrite (TF-15), and updated ages for TF-10, TF-11, TF-12 and TF-13 tephras at Fucino (Table 1). Specifically, these Fucino ash layers were correlated to the Triflisco, Cancello, Montemaoro/X-5 and Maddaloni/X-6 tephra (Giaccio et al., 2017), sourced in Campi Flegrei (Monaco et al., 2022b) and dated to 91.8 ± 1.2 ka/93.0 ± 0.4 ka (Monaco et al., 2022b; Fernandez et al., 2024), 102.5 ± 0.8 ka (Monaco et al., 2022b), 105.6 ± 0.5 ka/106.2 ± 0.4 ka (Petrosino et al., 2016; Fernandez et al., 2024) and 109.1 ± 0.8 ka/109.3 ± 1.0 ka (Regattieri et al., 2015; Monaco et al., 2022b), respectively. The age model and corresponding 95 %-confidence interval were calculated with *Bacon* software (Blaauw and Christen, 2011) written in the open-source statistical environment R (R Core Team, 2022).

3.4. Pollen and non-pollen palynomorph analysis

A total of 376 samples between 47.87 and 63.89 bbf m of the F1-F3 sequence were prepared for palynological analysis. A regular sampling interval of 4 cm was employed, equivalent to a mean temporal resolution of ~80 years based on an average sediment accumulation rate of ~5 mm yr^{-1} during the LIG. Prior to preparation, tablets of *Lycopodium clavatum* spores were added to each 1 cm^3 sample to determine pollen concentration and accumulation rates (Stockmarr, 1971). Following standard procedures, the samples were treated with hot 10 % HCl, 10 % KOH, 40 % HF and an acetolysis mixture (Fægri and Iversen, 1989; Moore et al., 1991; Bennett and Willis, 2001) (see Supplementary Methods).

Individual pollen grains were examined using a Leica DM2000 microscope at 400x magnification with a systematic counting method employed to obtain a minimum of 300 identifiable terrestrial pollen grains per sample (Birks and Birks, 1980; Seppä, 2013). Distinctive morphological features were inspected using 1000x magnification and identifications informed by reference collections and literature (Fægri and Iversen, 1989; Moore et al., 1991; Reille, 1999; Beug, 2004). A distinction was made for *Quercus* pollen grains, grouping taxa into the classification of Blaauw and Christen (2011): *Quercus robur*-type (deciduous oaks), *Quercus ilex*-type (evergreen oaks except *Quercus suber*) and *Quercus cerris*-type (semi-deciduous oaks and *Quercus suber*). Indeterminate grains, aquatic pollen and spores from pteridophytic vascular plants and bryophytes were counted but excluded from the terrestrial pollen sum (Cushing, 1967; Van Geel, 2001). Algal remains were identified with reference to selected literature and, owing to their abundance, counted until a minimum of 300 pollen grains was reached (Jankovská and Komárek, 2000; Komárek and Jankovská, 2001; Hillbrand et al., 2014). Absolute pollen and charcoal concentrations (cm^{-3}) were determined based on the marker grain method using *Lycopodium* counts (Stockmarr, 1971). Pollen and charcoal concentrations were converted into accumulation rates (cm^{-2} yr^{-1}) using the sedimentation rate. Owing to the non-laminated nature of the sedimentary record and large areal extent of the Fucino Basin, each data point in the pollen record is interpreted as representing pollen production over a period of several years averaged across the pollen source area.

Pollen taxa percentages were grouped into summary groups to illustrate key trends. Arboreal pollen, comprising all trees and shrubs, was further divided into groups reflecting species environmental preferences: pioneers (*Betula, Hippophae, Juniperus, Pinus* and *Salix*); temperate trees (arboreal taxa excluding pioneer species and *Cedrus*), Mediterranean sclerophylls (*Olea, Phillyrea,* and *Pistacia*; evergreen *Quercus ilex*-type was excluded from the Mediterranean grouping because of the broader range of Mediterranean climates it occupies and intolerance to extreme drought compared to other sclerophyllous species (Terradas, 1999); non-arboreal pollen (all herbs and Ericaceae), semi-desert (Amaranthaceae and *Artemisia*). Additional herb communities include heliophilous (Asteroideae, *Centaurea,* Cichorioideae, *Helianthemum, Plantago* and *Urtica*), thermophilous (Fabaceae and Lamiaceae) and hygrophilous (Cyperaceae, *Polygonum* and *Thalictrum*) taxa.

3.5. Microscopic charcoal analysis

Micro-charcoal particles were counted on the same analysed pollen slides at 400x magnification until a minimum of 200 *Lycopodium* spores had been reached, a counting sum considered sufficient to reliably reconstruct fire incidence with low error (Tinner and Hu, 2003; Finsinger and Tinner, 2005). The inclusion of charcoal particles was restricted to black, angular and entirely opaque fragments of at least 10 μm diameter (Swain, 1973; Clark, 1988). Similarly to the pollen record, each data point in the charcoal influx record is interpreted as representing the quantity of biomass burning over a period of several years averaged across the entire catchment.

3.6. $\delta^{18}O$ bulk carbonate analyses

Bulk carbonate $\delta^{18}O$ was measured with an Analytical Precision AP2003 spectrometer every ~8 cm (~160-year resolution) on a total of 166 samples from F1-F3 (47.87–63.89 bbf m; ~138.6 to 107.3 ka) by analysing the isotopic composition of evolved $CO_{2(g)}$ following acid reaction (see Supplementary Methods). Normalisation and calibration of the samples to the Vienna Pee Dee Belemnite (V-PDB) scale was conducted using a set of internal standards. The internal standard has a mean analytical precision (1σ) of ±0.10 ‰ and the average analytical precision (2σ) of samples is recorded at ± 0.18 (Mannella, 2020; Mannella et al., 2020). Mannella et al. (2020) showed that different methods of pre-treatment to remove organic matter introduced minor but unpredictable isotopic effects and therefore pre-treatment was not employed on Fucino samples.

Table 1
Constraining the late Penultimate Glacial to early Last Glacial chronology of F1-F3. The tephra-free depth below basin floor (bbf) of tephra layers and cryptotephras is provided. Geological units and correlative tephra identifications, age (ka ± 2σ) and dating method are based on the references. Cryptotephra TF-14-C1 has not been used as a control point in the age model. The new ages for the Vico C Ignimbrite and Vico B Ignimbrite, correlative with TF-15 and TF-16, respectively, are given.

Marker	Depth bbf base (m)	Unit/Correlative (s)	Input $^{40}Ar/^{39}Ar$ age (ka ± 2σ)	Dating method	Age-depth model	Modelled age (ka ± 2σ)	Reference
TF-10	41.10	Triflisco	91.8 ± 1.4	$^{40}Ar/^{39}Ar$	included	92.3 ± 1.8	Monaco et al. (2022b)
TF-11	45.41	Cancello/TM-24b	102.5 ± 0.8	$^{40}Ar/^{39}Ar$	included	102.3 ± 0.9	Monaco et al. (2022b)
TF-12	47.13	Montemaoro/X-5	105.6 ± 0.5	$^{40}Ar/^{39}Ar$	included	105.7 ± 0.6	Petrosino et al. (2016)
TF-13	48.62	Maddaloni/X-6	109.1 ± 0.8	$^{40}Ar/^{39}Ar$	included	108.9 ± 1.0	Regattieri et al. (2015)
TF-14	57.31	Sabatini/TM-36	126.0 ± 1.0	$^{40}Ar/^{39}Ar$	included	126.0 ± 1.3	Giaccio et al. (2017)
TF-14-C1	59.50	LGdM TM-42	132.1 ± 6.6	Varve age	not-included	130.2 ± 2.0	Wulf et al. (2012)
TF-15	65.96	Vico C	142.6 ± 0.4	$^{40}Ar/^{39}Ar$	included	142.7 ± 0.6	This study
TF-16	69.81	Vico B	151 ± 0.7	$^{40}Ar/^{39}Ar$	included	150.9 ± 1.0	This study

3.7. Data analyses (see Supplementary Methods)

Stratigraphic diagrams were created using C2 1.7.7 (Juggins, 2007) and pollen, algal and fungal spore taxa ordered according to appearance and dominance in the stratigraphic record. Temporal changes in vegetation succession are displayed using Pollen Assemblage Zones (PAZs). Numerical zonation was derived using optimal splitting by information content to analyse down-core changes and capture floristic shifts in PSIMPOLL 4.26 (Bennett, 2008) (see Supplementary Methods). The rate of change (RoC) of the F1-F3 late Penultimate Glacial to early Last Glacial pollen and algal records was calculated using the *R-Ratepol* package (Mottl et al., 2020) to quantitatively analyse taxonomic responses to environmental changes (see Supplementary Methods). RoC provides a metric for community turnover by estimating the magnitude of compositional change. The presence of rapid change in community structure was defined by 'peak points' based on a significant increase in RoC score using a non-linear trend (Mottl et al., 2021). Multivariate analyses were conducted using CANOCO 5 to investigate vegetation responses in the pollen assemblage (Ter Braak and Šmilauer, 2018) (see Supplementary Methods). A total of 45 pollen taxa, expressed as percentage abundance, were used in multivariate analyses of the late Penultimate Glacial to early Last Glacial. Rare species with <5 occurrences and <2 % maximum abundance were excluded. Principle Component Analysis (PCA) was performed following Detrended Correspondence Analysis (DCA) revealing a homogenous, linear response of the vegetation community (DCA axis 1 gradient length = 2.4 SD) (Šmilauer and Lepš, 2014). To detect the fingerprint of abrupt climate events, the temperate tree pollen and charcoal data were detrended and smoothed (see Supplementary Methods).

The offset ($\Delta\delta^{18}O$) between the $\delta^{18}O$ records from Fucino Basin and the speleothem stack of Corchia Cave in the Alpi Apuane karst (Fig. 1), Italy, was used as a proxy for the evaporative regime at Fucino. The $\delta^{18}O$ records were initially interpolated using a 1-year time window to account for different age scales and resolutions (Tzedakis et al., 2018). A moving average was then applied to the interpolated datasets using the *gtools* package (Bolker et al., 2022) with a defined window spanning 100 consecutive points. The isotopic difference between the records was calculated by subtracting the smoothed Fucino $\delta^{18}O$ record from the smoothed Corchia $\delta^{18}O$ values (see Supplementary Methods).

4. Results

4.1. Chronology

4.1.1. $^{40}Ar/^{39}Ar$ dating

A total 14 sanidine crystals from Vico B Ignimbrite, 10 sanidine crystals from Vico C Plinian and 20 leucite and sanidine from Vico C Ignimbrite were dated (Fig. 4). Full analytical details are provided in Supplementary Methods. The 14 crystals from Vico B gave a weighted mean age of 151.0 ± 0.5 ka (2σ) (1.4 ka, MSWD = 1.5, p = 0.1). The 10

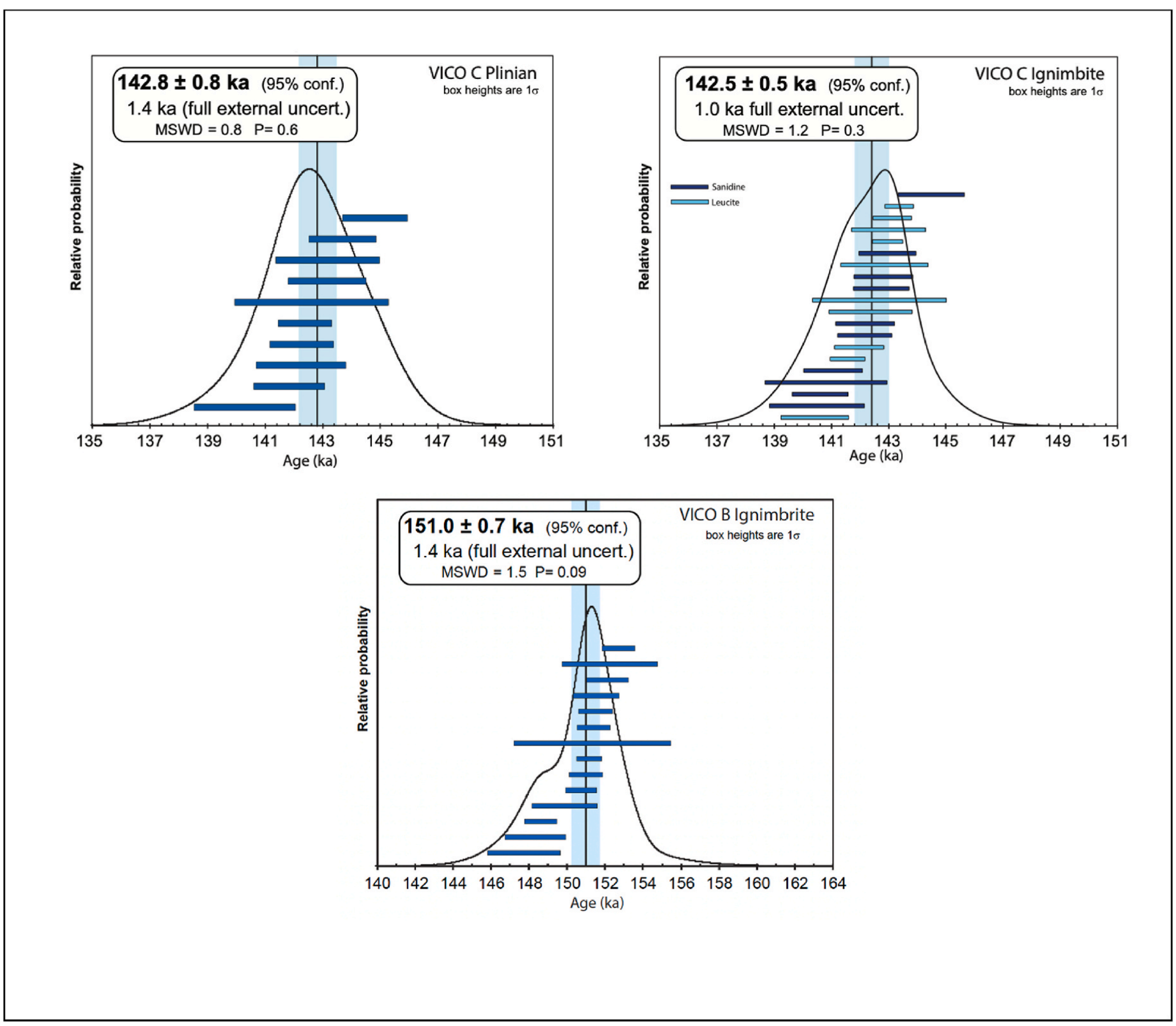

Fig. 4. Age probability density spectra diagrams for Vico C Plinian and Vico C Ignimbrite as well as Vico B Ignimbrite. Dark blue bars = sanidine crystal and light blue bars = leucite crystal.

sanidine crystals from the Vico C Plinian subunit display uniform age agreement within uncertainties, producing a weighted mean age of 142.8 ± 0.8 ka (2σ) (1.4 ka, MSWD = 0.8, p = 0.6) (Fig. 4). For the Vico C Ignimbrite, the 20 crystals produced a weighted mean age of 142.5 ± 0.5 ka (2σ) (1.0 ka, MSWD = 1.2, p = 0.3). The combined age of the co-eruptive Plinian and Ignimbrite Vico C sub-units yielded a weighted mean age of 142.6 ± 0.4 ka, which here is taken as the best determination. As previously mentioned, Giaccio et al. (2017) considered TF-15 and TF-16 as distal equivalents of the Vico C Ignimbrite and Vico B Ignimbrite, respectively, based on similar glass compositions.

The new $^{40}Ar/^{39}Ar$ dates for the Vico B (151.0 ± 0.7 ka) and C (142.5 ± 0.5 ka) Ignimbrites are significantly different from the previous $^{40}Ar/^{39}Ar$ ages of 157 ± 3 (2σ) ka and 151 ± 1 (2σ) ka, respectively, obtained by Laurenzi and Villa (1987) for the same volcanic units. The absence of a reference age for the standard (B4M) used by Laurenzi and Villa (1987) makes it challenging to evaluate whether a difference in $^{40}Ar/^{39}Ar$ ages could be a result of more accurate recent calibrations. Furthermore, there is the potential for xenocrystic contamination in the methodology of Laurenzi and Villa (1987), which has been shown to yield older ages as opposed to using juvenile sanidine phenocrysts (Spell et al., 2001).

4.1.2. Cryptotephra identification, analysis, and correlation (TF-14-C1)

Glass shard counts in the low-resolution samples (continuous 5 cm intervals) from the F1-37 core section reveal cryptotephra spanning 120–135 cm, with no glass shards observed in the remaining portions of the F1-37 core section (Fig. S1). Counts in the high-resolution (1 cm) samples taken across the 120–135 cm interval constrained the position of the relatively diffuse cryptotephra layer to 126–133 cm. This cryptotephra in the F1-37 core section is herein named TF-14-C1 and it comprises a distinctive double peak in glass shard concentrations (Fig. S1). The lowermost peak occurs at 132–133 cm (tephra-free depth 59.54–59.55 bbf m) where shard concentrations were 3068 shards/gram (herein referred to as TF-14-C1a; Fig. S1; Table S1). The stratigraphically higher peak is located between 126 and 127 cm (tephra-free depth 59.49–59.50 bbf m), it displays higher concentrations of glass shards (4626 shards/g) and is referred to as TF-14-C1b (Table S1).

Glass shards from both cryptotephra peaks, TF-14-C1 (TF-14-C1a [lower] and TF-14-C1b [upper]), display a geochemically indistinguishable phono-trachytic glass composition (Fig. S2). Given that both peaks are geochemically identical, they are interpreted to be associated with the same eruption, the lower peak reflecting an initial ash fall event (TF-14-C1a) and the upper peak (TF-14-C1b) reflecting reworking/inwash of glass shards from within the Fucino catchment. Consequently, the isochron is placed at 132–133 cm (Tephra-free depth 59.55 bbf m).

The low-alkali ratio ($Na_2O > K_2O$) phono-trachytic glasses of cryptotephra TF-14-C1 are entirely consistent with the eruptive products of Ischia Island situated in the Bay of Naples, Italy (Fig. S2). The chronostratigraphic position of TF-14-C1 above the visible tephra TF-15/Vico C (142.6 ± 0.4 ka; this study) and below TF-14 (126 ± 1.0 ka; Giaccio et al., 2017), combined with the available geochemical proxies and age-depth model (Giaccio et al., 2017; Mannella et al., 2019) place the cryptotephra in the late MIS 6 glacial period (Mannella et al., 2019). The eruptive history of Ischia during the corresponding time-interval is poorly constrained due to limited lon and exposure on the island. Thus, the glass chemistry of TF-14-C1 is compared to ash layers preserved in the 133 ka-long sedimentary succession of Lago Grande di Monticchio (LGdM) situated ~100 km east of Ischia, which provides a detailed distal record of activity at Ischia and other Italian volcanoes (Wulf et al., 2004, 2012; Tomlinson et al., 2014). To identify potential correlatives of the TF-14-C1 cryptotephra in the LGdM sequence, we considered layers with Ischia-type chemical compositions which occur in the correct climato-stratigraphic position. At LGdM, only two Ischia-type layers reside in the late MIS6, TM-40 (~131 ka) and TM-42 (~132 ka), both of which have independent ages, albeit with relatively large uncertainties (±~6 ka; Wulf et al., 2012). Despite the similar phono-trachytic glass chemistries observed in both LGdM layers, overall, the chemical data would point to a correlation between TF-14-C1 and the chemically homogeneous TM-42, the oldest tephra in the LGdM succession (Fig. S3a–b; see Supplementary Methods). Regardless of the imprecise varve age of TM-42, this tephra correlation provides a potentially important chronological tie-point capable of directly synchronising the Fucino and LGdM proxy records immediately prior to the transition into the LIG.

4.1.3. Age-depth model

The depth distribution of the updated and new $^{40}Ar/^{39}Ar$ dating, used as input ages for developing the Bayesian age-depth model, is virtually linear and the resulting age-depth curve shows a very homogenous sedimentation rate (Fig. 5). The combination of high-precision $^{40}Ar/^{39}Ar$ ages and the linear trend of the age control points yields a very small uncertainty of the resulting modelled ages, which is ±1.7 ka on average and ranges between ±1.0 ka and ±2.2 ka at 2σ error (Fig. 5; Supplementary dataset S2), thus providing a robust and precise chronology for the Fucino MIS 6-MIS 5b proxy records.

4.2. Pollen stratigraphy

A total of 99 pollen and spore taxa encompassing angiosperms, gymnosperms and pteridophytes were identified in the 375 samples from the late Penultimate Glacial to early Last Glacial F1-F3 sequence from the Fucino Basin. Of the 84 taxa included in the pollen sum, 26 tree taxa, 7 shrub taxa, Ericaceae and 50 herbaceous taxa were recorded. Pollen grains were largely very well-preserved and the percentage of indeterminate grains ranged between 2 and 12 % (average = 5 %). The main features of the pollen records are illustrated in Fig. 6 with the dominant vegetation outlined in Table 2.

Fig. 6 (continued) Shown are the most abundant herb and aquatic taxa with exaggeration curves (10x) alongside summary vegetation groups (Non-arboreal and Semi-desert) and non-pollen palynomorph algal remains (%) with PAZs displayed.

In the Principal Components Analysis (PCA) of pollen samples, the first two axes explain 47 % of species variation at Fucino during the late Penultimate Glacial to early Last Glacial (Fig. 7; Table 4). PCA axis 1, accounting for 34 % of the variation, distinguishes samples based on the dominance of herbaceous or temperate taxa. Older samples in pollen zones F1-F3-6-1, F1-F3-6-2, F1-F3-6-3 and F1-F2-6-4 have greater proportions of plants such as Amaranthaceae, *Artemisia* and Poaceae, and hence higher values along the first PCA axis. In contrast, pollen samples in zones F1-F3-5-1 to F1-F3-5-4 are dominated by temperate tree taxa, including *Q. robur*-type, *C. betulus* and *O. carpinifolia/C. orientalis*. Species assemblages along PCA axis 2, explaining 13 % of variation, appear determined by proportions of aquatic communities and Mediterranean sclerophylls indicative of summer aridity compared to arboreal taxa with high moisture requirements and/or adapted to seasonally cold climates. While zone F1-F3-5-1 is distinct in its high proportions of aquatic taxa, including *Myriophyllum* and *Sparganium/T. angustifolia* and the herbaceous family Ranunculaceae, elevated abundances of Mediterranean taxa characterise zone F1-F3-5-2. Zones F1-F3-5-6 to F1-F3-5-10 are dominated by *Abies, Alnus, Betula, Buxus, Picea* and *Pinus* and thus have low PCA axis 2 scores.

4.3. Pollen and charcoal correlation

To compare the relationship between pollen summary groups and charcoal accumulation rate during glacial-interglacial transitions and within the LIG, the F1-F3 succession was separated into the entire investigated interval of the late Penultimate Glacial to early Last Glacial (~138.6–107.3 ka) and the pollen-based LIG only (~129.2–108.8 ka) (Table 3) (See Supplementary Methods). During the entire investigated period, significant positive correlations occur between CHAR and temperate (0.20) and Mediterranean taxa (0.34) (Table 4). In contrast,

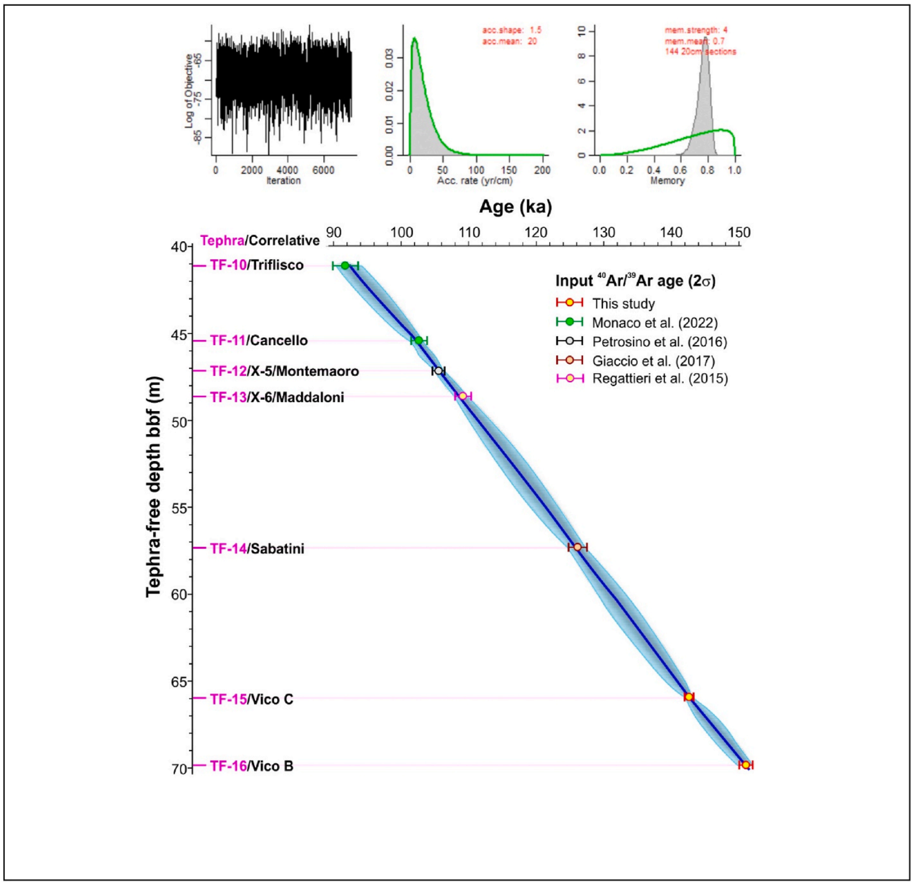

Fig. 5. Age model for F1-F3 plotted against composite tephra-free depth below basin floor (bbf) (m). The input $^{40}Ar/^{39}Ar$ ages (2σ) for the identified tephra layers are shown.

the strongest negative correlation exists between charcoal influx and pioneer vegetation (−0.43). Correlations between charcoal influx and arboreal, non-arboreal and semi-desert taxa are not statistically significant. A higher positive correlation occurs between CHAR and Mediterranean taxa (0.40) when considering the LIG period only. Positive correlations also exist between charcoal influx and non-arboreal (0.23) and semi-desert (0.19) vegetation. A negative relationship is apparent between CHAR and pioneer (−0.30) and arboreal (−0.23) taxa. In contrast to the entire investigated period, an insignificant correlation occurs between charcoal influx and temperate vegetation within the LIG.

4.4. The $\delta^{18}O_c$ record

The late part of the Penultimate Glacial is characterised by almost invariant $\delta^{18}O_c$ values of ca. −3 ‰ until 129.5 ka (Fig. 8). Short intervals of higher $\delta^{18}O_c$ are present at ~132 ka and 134 ka. The $\delta^{18}O_c$ values then progressively decrease to −5 ‰ at 125 ka, reaching minimum values at ~124 ka, with a final step of more than −1 ‰. Then $\delta^{18}O_c$ values progressively increase again with a period of near-invariant values from ~117 to 114 ka. At ~111 ka, the values increase for ~2 ka.

5. Discussion

5.1. Long-term vegetation and environmental changes

5.1.1. The Penultimate Glacial

The late Penultimate Glacial at Fucino Basin (138.6 ± 2.1 ka to 129.2 ± 1.9 ka) was an interval of open steppe vegetation characterised by Amaranthaceae, *Artemisia* and Poaceae and limited pollen productivity (PAR: 15–107 × 10^5 grains cm^{-2} yr^{-1}) (Table 2; Fig. 6). Arboreal assemblages were characterised by *Betula, Juniperus* and *Pinus,* indicative of a mixed wooded steppe landscape. Tolerant of cold and arid conditions, this vegetation composition suggests severe moisture deficiency and cool seasonal temperatures (Brauer et al., 2007; Pickarski et al., 2015). The low vegetation cover and cold conditions are also reflected by depleted CHAR values and hence low levels of biomass burning (Lawson et al., 2013). A transition from the dominance of Poaceae to the semi-desert taxon *Artemisia* implies increased aridity between 134.7 ± 2.1 ka and 130.6 ± 2.1 ka. A notable feature of the record is the occurrence of *Q. robur*-type and *Ulmus* at low abundances, and the sporadic presence of several temperate tree taxa including *Fagus*. This signifies the presence of small refugial temperate tree populations in the Central Apennines during the Penultimate Glacial. The relatively high orographic precipitation of the Central Apennines and the presence of Fucino lake (with its heat capacity) likely provided adequate moisture to sustain thermophilous trees during arid climates and suitable habitats in the topographically varied catchment. Overall, the combination of dominant steppe vegetation, minor arboreal abundances and limited fire activity indicates a cold continental climate and strong aridification during the late Penultimate Glacial.

Algal community assemblages offer supporting evidence, tracking changing hydrologic conditions. In alignment with the palynological record, a rapid algal community turnover occurred at 134.7 ± 2.1 ka from the highly abundant *P. simplex* var. *sturmii*, characteristic of relatively deep water and oligotrophic conditions, to a proliferation of numerous *Pediastrum* species, *Botryococcus* and *T. minimum* (Komárek and Jankovská, 2001; Whitney and Mayle, 2012). Elevated abundances of *Botryococcus* compared to *Pediastrum* occurred during the peak in *Pinus* at 133.7 ± 2.2 ka, reflecting more eutrophic or brackish conditions

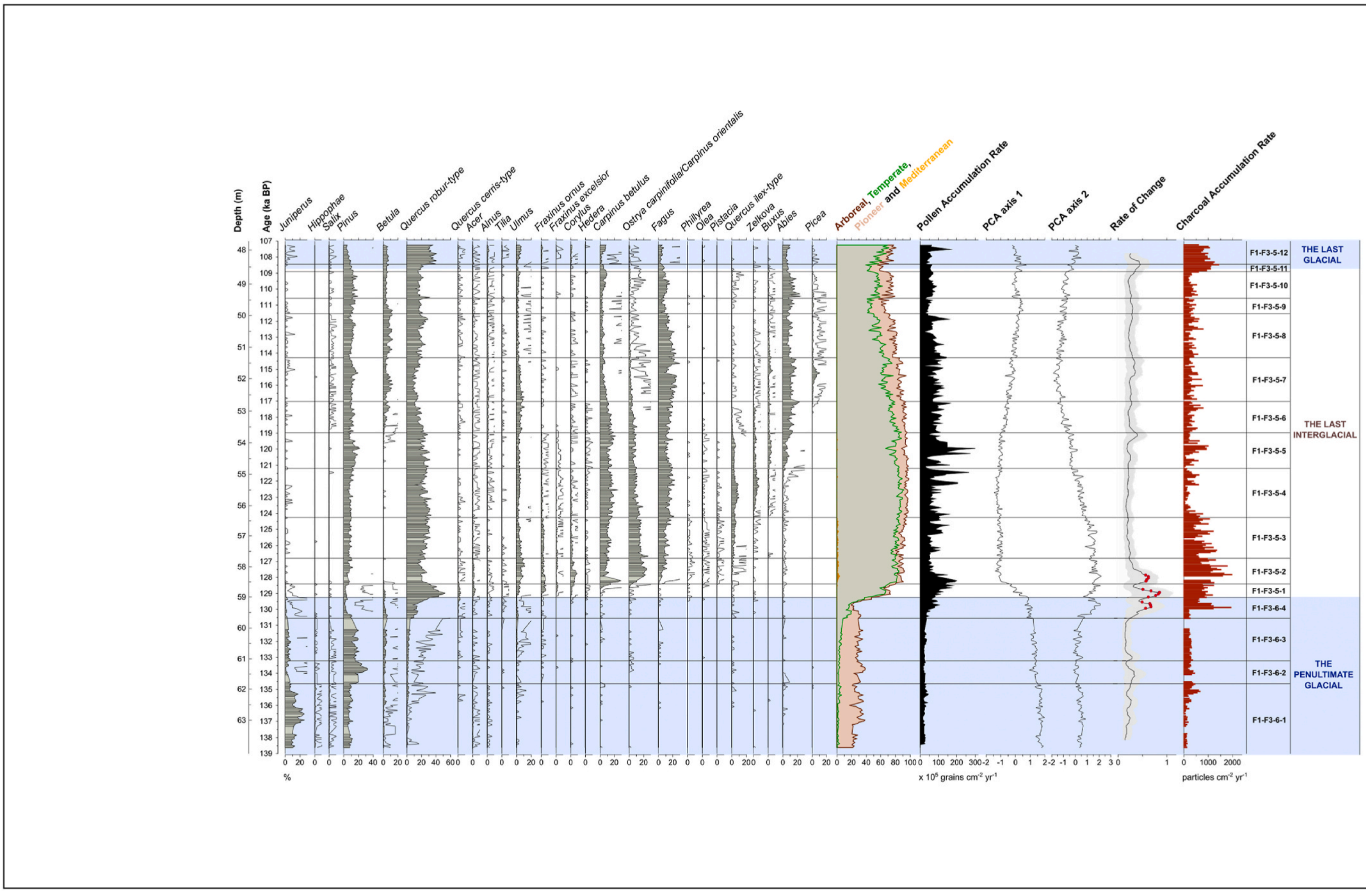

Fig. 6. Pollen diagram of the late Penultimate Glacial to early Last Glacial (~138.6–107.3 ka) at Fucino Basin. Most abundant tree and shrub taxa are displayed with exaggeration curves (10x) alongside summary vegetation groups (Arboreal, Temperate, Pioneer and Mediterranean) expressed as percentages (%). Pollen Accumulation Rate (PAR) (x10^5 grains cm^{-2} yr^{-1}), PCA axis 1 and 2 scores, RoC scores with detected peak points (red circles) and uncertainty (grey shading), Charcoal Accumulation Rate (CHAR) (particles cm^{-2} yr^{-1}) and Pollen Assemblage Zones (PAZs) are shown.

(Clausing, 1999; Negrini et al., 2006). Subsequent expansions of *T. minimum* from 133.6 ± 2.2 ka, followed by the thermophilic taxa *P. boryanum* var. *brevicorne* and *P. boryanum* var. *boryanum* indicates open water conditions and higher summer temperatures (Reynolds, 1984; Jankovská and Komárek, 2000; Komárek and Jankovská, 2001; Moss et al., 2003; Ralska-Jasiewiczowa et al., 2003; Niemeyer et al., 2015). The expansion of cold tolerant *P. kawraiskyi* between 132.8 ± 2.1 ka to 129.6 ± 1.9 ka signifies seasonally cooler temperatures during the glacial-interglacial transition (Nielsen and Sørensen, 1992; Komárek and Jankovská, 2001). The hydrological changes inferred from algal remains are supported by evidence on late Pleistocene glacier dynamics and lake level oscillations in the Central Apennines with higher (lower) lake levels associated with glacier advances (retreats). In this regard, meltwater and/or a reduced summer evaporative regime may have sustained Fucino lake level during arid glacial states (Giraudi, 1989, 1998; Giraudi and Frezzotti, 1997; Giraudi and Giaccio, 2015).

The transition to interglacial conditions documents increased *Q. robur*-type alongside a declining presence of *Artemisia,* Poaceae, *Juniperus* and *Pinus* from 130.6 ± 2.0 ka. A notable climatic return to colder and more arid conditions interrupted the transition between 130.0 ± 2.0 ka to 129.7 ± 1.9 ka, manifested across an array of ecological proxies. The replacement of arboreal vegetation cover (10 % decline) with steppe vegetation corresponds with an unprecedented expansion in aquatic plant communities, namely the obligate aquatic taxa *Myriophyllum* growing submerged in shallow freshwater and the rhizomatous herb *Sparganium/T. angustifolium* favouring lake margins, are indicative of lowered lake levels (Pignatti, 1982; Miola et al., 2006). Elevated abundances of the herbaceous family Ranunculaceae, comprising several species of an aquatic nature, and rapid expansion of the semi-desert indicator Amaranthaceae support the inference of a shallower lake. Concurrent drastic drops in algal taxa reflect a cool and dry interval unfavourable for reproduction.

5.1.2. *The Last Interglacial*

Characterised by a marked expansion of *Q. robur*-type at the expense of steppic herbaceous taxa, the pollen-based LIG onset at Fucino is recorded at 129.2 ± 1.9 ka when arboreal pollen surpasses 50 %, increasing from 20 % to 73 % in ~800 years (Table 2; Fig. 6). The temperate phase commenced with an early expansion of *Q. robur*-type indicating rising temperature and precipitation. The development of a floristically diverse temperate forest of *Ulmus, F. ornus, F. excelsior, Corylus, Tilia* and *Fagus* ensued. By 128.2 ± 1.8 ka, a peak in the meso-thermophilous *C. betulus* suggests cool winter conditions and increasing precipitation (Kühl and Litt, 2003; Sánchez Goñi et al., 2005). Subsequent expansion of *O. carpinifolia/C. orientalis* and Mediterranean sclerophylls *(Olea, Phillyrea* and *Pistacia)* occurred alongside enhanced hydrological seasonality, summer drought and frost-free winters during the period of maximum NH summer insolation (Tzedakis, 1994, 2007; Milner et al., 2012). Substantially increasing in step with temperate vegetation cover, charcoal influx was greatest during this first phase of elevated summer temperatures and seasonal moisture deficiency from 130.0 ± 2.0 ka to 124.0 ± 1.4 ka. The positive correlation between CHAR and temperate vegetation observed on a glacial-interglacial timescale suggests the elevated biomass of the LIG forest supplied a

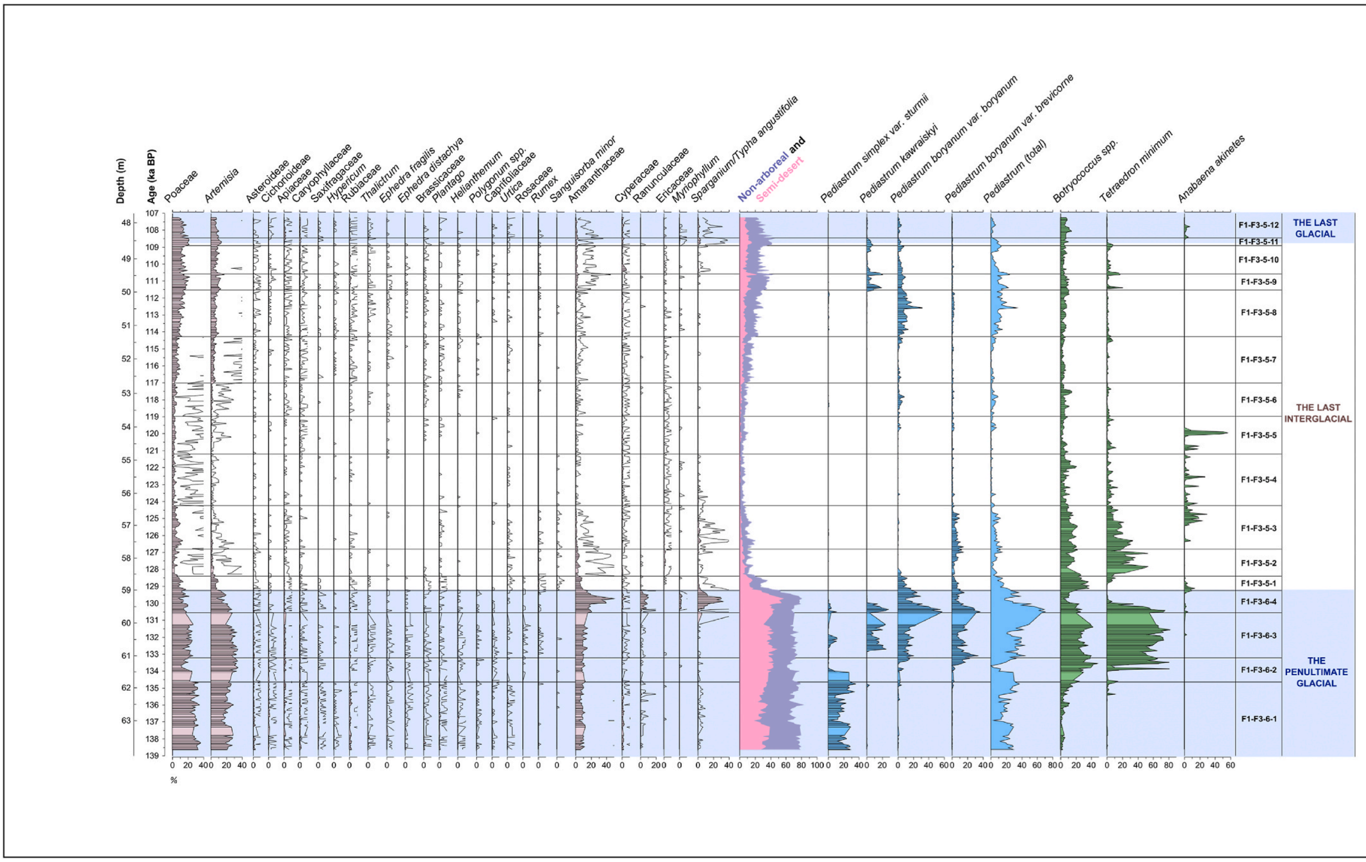

Fig. 6. (*continued*).

greater fuel load. An additional control on fire activity appears to be summer conditions as indicated by the strongest positive correlation displayed between CHAR and Mediterranean taxa during the LIG (Turner et al., 2008; Lawson et al., 2013). Moreover, an increased abundance of *Botryococcus* at the expense of *Pediastrum* reflects warmer, shallower and more eutrophic conditions (Guy-Ohlson, 1992; Rull et al., 2008). A substantial *T. minimum* community, particularly during the early stages from 127.9 ± 1.7 ka to 127.0 ± 1.6 ka, correlates with high NH summer insolation (Reynolds, 1984; Clausing, 1999; Ralska-Jasiewiczowa et al., 2003; Niemeyer et al., 2015). Fossil akinetes of the nitrogen-fixing *Anabaena*-type cyanobacteria were present in abundance from 125.4 ± 1.7 ka and indicate high temperatures and nitrogen-limited conditions (Van Geel et al., 1994; Paerl and Huisman, 2009; Rasconi et al., 2015).

Following this interval of elevated summer aridity, arboreal pollen values reached a maximum of 98 % between 124.2 ± 1.7 ka and 119.0 ± 2.2 ka with *Q. robur*-type and *C. betulus* remaining abundant. Extensive communities of late-successional, humid-demanding species including *Fagus* and later *Abies,* in addition to the cool-temperate evergreen, *Buxus*, developed as summer insolation declined and climate seasonality reduced (Tzedakis, 1994, 2007). The later peak in *Q. ilex*-type pollen (around 123.0 ± 1.9 ka) may reflect a local population expansion on sites of southern exposure as found in the catchment today (Lubell et al., 1995; De Sillo et al., 2012). In addition, although evergreen oaks are typically associated with summer aridity, *Q. ilex* is typically less drought-tolerant compared to characteristically aridity-resistant species such as *Q. coccifera* (Peguero-Pina et al., 2009; Petroselli et al., 2013; López-Tirado et al., 2018). Lowered charcoal quantities and a negative correlation between LIG arboreal cover and charcoal influx reflect reduced summer aridity and increased humidity (Lawson et al., 2013). The dominance of cyanobacteria suggests high temperatures and organic matter input, providing intensive nutrient loading and a competitive advantage over other phytoplankton taxa with concurrent loss in algal community diversity (Elliott et al., 2006; Paerl and Huisman, 2009).

A steady decline in temperate tree taxa was observed from 119.0 ± 2.2 ka as the pioneer tree *Betula* and steppe communities of predominantly Poaceae and *Artemisia* became re-established. A transient establishment of *Picea* with proportions of 11 % by 115.3 ± 2.1 ka indicates a local presence in the surroundings of the Fucino Basin under favourable cold and moist conditions (Huntley and Birks, 1983; Ravazzi, 2002; Giesecke and Bennett, 2004). Elevated abundances of *Abies* from 119.0 ± 2.2 ka to 114.3 ± 2.1 ka, a taxon generally limited to moist mountainous habitats with a more localised pollen source area, as well as mesothermic *Buxus*, peaking at 6 % by 115.1 ± 2.1 ka, support the inference of a cooler, more humid climate (Tzedakis, 2007; Alba-Sánchez et al., 2010). A post-temperate phase of open woodland ensued as temperate trees reached a LIG minimum of 42 % at 111.5 ± 1.7 ka. Several contractions in temperate vegetation occurred during this period reflecting deteriorating conditions related to millennial-scale variability. The dominance of *Pediastrum* communities over *Botryococcus* indicates oligotrophic conditions with transitions to a cooler climate inferred from expansions of *P. kawraiskyi* at 111.4 ± 1.6 ka, 110.6 ± 1.5 ka and 108.9 ± 0.9 ka (Jankovská and Komárek, 2000; Komárek and Jankovská, 2001). Fire activity rapidly increased from 109.0 ± 1.0 ka, as NH summer insolation strengthened. Increased values of CHAR and non-arboreal and semi-desert taxa during the forested interval suggest peak charcoal production may have occurred during intermediate aridity levels with sufficient biomass (Krawchuk and Moritz, 2011; Lawson et al., 2013).

5.1.3. The early Last Glacial

The onset of the early Last Glacial is marked by a decline in arboreal pollen values to 58 % and an increase in Poaceae and *Artemisia* at 108.8

Table 2
Description of the dominant biome (based on characteristic plant functional types identified by Prentice et al., 1996, main palynological characteristics (minimum to maximum %), Pollen Accumulation Rate (PAR) (x 10^5 grains cm^{-2} yr^{-1}), algal communities (minimum to maximum %) and Charcoal Accumulation Rate (CHAR) (particle cm^{-2} yr^{-1}) for the sixteen Pollen Assemblage Zones (PAZs) for the late Penultimate Glacial to early Last Glacial (~138.6–107.3 ka) at Fucino Basin.

PAZ F1-F3	Dominant biome	Main palynological characteristics (minimum to maximum %)	PAR (x 10^5 grains cm^{-2} yr^{-1})	Algal communities (minimum to maximum %)	CHAR (particles cm^{-2} yr^{-1})
6–1 (63.9–61.8 m; 138.6–134.7 ka; 3900 years)	Steppe/ desert	Dominance of non-arboreal pollen. **AP (17–39 %):** *Juniperus* was a major component (4–26 %). **NAP (61–83 %):** High values of Poaceae (20–36 %) and *Artemisia* (13–29 %).	Low stable PAR (15–48).	Dominated by *P. simplex* var. *sturmii* (3–36 %).	Low increasing CHAR (52–699).
6–2 (61.8–61.1 m; 134.7–133.2 ka; 1500 years)	Steppe/ desert	High abundances of steppe pollen taxa and expansion of *Pinus*. **AP (23–39 %):** Expansion of *Pinus* (16–33 %). Reduced *Juniperus* values (1–7 %). **NAP (61–77 %):** *Artemisia* dominated (24–35 %). Poaceae values declined (11–25 %).	Low stable PAR (17–30).	Expansion of *Botryococcus* (17–48 %), *T. minimum* (0–81 %), *P. boryanum* var. *brevicorne* (0–23 %) and *P. boryanum* var. *boryanum* (0–16 %).	Low stable CHAR (191–475).
6–3 (61.1–59.7m; 133.2–130.6 ka; 2600 years)	Steppe/ desert	Dominance of steppe pollen and *Pinus*. **AP (24–35 %):** *Pinus* remained abundant (10–21 %), *Betula* (1–6 %) and *Q. robur*-type (1–5 %) gradually increased. **NAP (65–76 %):** *Artemisia* dominant (19–34 %). High values of Poaceae (13–27 %).	Low stable PAR (19–37).	Diverse community of *Pediastrum* (20–66 %), *Botryococcus* (20–42 %) and *T. minimum* (44–82 %).	Low stable CHAR (225–399).
6–4 (59.7–59.0 m; 130.6–129.2 ka; 1400 years)	Steppe/ desert	Substantial expansion in herb and aquatic pollen taxa. **AP (20–48 %):** Increasingly high percentages of *Q. robur*-type (9–31 %). **NAP (52–80 %):** Expansion driven by Amaranthaceae (14–50 %) and Ranunculaceae (<11 %). **Aquatic:** Large increase in *Sparganium/T. angustifolium* (0–30 %) and *Myriophyllum* (<4 %).	Moderate increasing PAR (32–107).	Rapid declines in *Pediastrum* (18–70 %), *Botryococcus* (3–28 %) and *T. minimum* (0–75 %).	Moderate-high increasing CHAR (221–1974).
5–1 (59.0–58.6 m; 129.2–128.4 ka; 800 years)	Temperate woodland	Shift in a dominance of steppe to arboreal taxa. **AP (58–79 %):** *Q. robur*-type peaked and became the dominant taxon (32–53 %). **NAP (21–42 %):** Further decreases in the presence of Poaceae (6–17 %), *Artemisia* (4–9 %) and Amaranthaceae (5–9 %).	High increasing PAR (80–183).	Further contractions in *Pediastrum* (8–24 %), expansion of *Botryococcus* (22–37 %) and *Anabaena* akinetes (0–13 %).	Moderate-high increasing CHAR (764–1248).
5–2 (58.6–57.7 m; 128.4–126.8 ka; 1600 years)	Mixed forest	Expansion of temperate arboreal taxa. **AP (81–92 %):** *C. betulus* peaked (4–29 %), replaced by *O. carpinifolia/C. orientalis* (6–24 %) and *Q. robur*-type (15–28 %). Increase in *Ulmus* (5–11 %), *Fagus* (1–12 %) and *Corylus* (1–9 %). Expansion of Mediterranean taxa (<5 %). **NAP (8–19 %):** Low steppe pollen values.	PAR peaked before declining (45–202).	Diminished *Pediastrum* populations (2–12 %), primarily *P. boryanum* var. *brevicorne* (1–12 %), expansion of *T. minimum* (8–53 %).	High CHAR, peaks before declining (702–2005).
5–3 (57.7–56.4 m; 126.8–124.2 ka; 2600 years)	Mixed forest	Increasing *Q. ilex*-type abundance. **AP (80–95 %):** *Q. robur*-type dominated (18–32 %) with substantial percentages of *O. carpinifolia/C. orientalis* (10–26 %), *C. betulus* (6–16 %) and *Fagus* (7–18 %). *Q.* ilex-type values increased (1–6 %). **NAP (5–20 %):** Small expansions in Poaceae (3–13 %).	Moderate fluctuating PAR (38–125).	Stable algal communities of *P. boryanum* var. *brevicorne* (0–15 %) and *Botryococcus* (8–22 %), gradual decline in *T. minimum* (3–33 %), rapid expansion of *Anabaena* akinetes (0–30 %).	Moderate declining CHAR (418–1379).
5–4 (56.4–54.9 m; 124.2–121.2 ka; 3000 years)	Mixed forest	Elevated abundance of *Fagus, Q. ilex*-type and *Zelkova*. **AP (92–98 %):** *Q. robur*-type remained most abundant (12–33 %) alongside *C. betulus* (11–24 %), *Fagus* (10–23 %) and *O. carpinifolia/C. orientalis* (5–19 %). *Q. ilex*-type peaked (3–10 %) with expansions in *Zelkova* (<8 %). **NAP (2–8 %):** Low steppe pollen values.	Moderate-high fluctuating PAR (46–270).	*Pediastrum* largely absent (<5 %), depleted populations of *Botryococcus* (1–21 %) and *T. minimum* (0–14 %), fluctuating expansion of *Anabaena* akinetes (0–27 %).	Low fluctuating CHAR (64–817).
5–5 (54.9–53.7 m; 121.2–119.0 ka; 2200 years)	Mixed forest	Expansion of *Abies* and *Buxus*. **AP (88–98 %):** Contractions in *Fagus* (9–20 %), *C. betulus* (8–21 %), *O. carpinifolia/C. orientalis* (3–10 %), *Q. ilex*-type (1–6 %) and *Zelkova* (1–5 %). Expansions in *Pinus* (7–21 %) *Buxus* (0–5 %) and *Abies* (2–13 %). **NAP (2–12 %):** Low steppe pollen values.	Moderate-high fluctuating PAR (29–303).	Reduced algal community diversity, fluctuating expansions of *Anabaena* akinetes (0–56 %).	Low-moderate fluctuating CHAR (43–1028).
5–6 (53.7–52.7 m; 119.0–117.0 ka; 2000 years)	Mixed forest	Expansions of *Betula* and *Abies*. **AP (88–96 %):** Decline in *Q. robur*-type (11–23 %), *C. betulus* (9–19 %) and *O. carpinifolia/C. orientalis* (2–11 %). *Betula*	Moderate fluctuating PAR (53–165).	Small populations of *P. boryanum* var. *boryanum* (<9 %), *P. boryanum* var. *brevicorne* (<4 %), *Botryococcus* (3–15 %) and *T. minimum* (<6 %).	Low fluctuating CHAR (136–821).

(continued on next page)

Table 2 (*continued*)

PAZ F1-F3	Dominant biome	Main palynological characteristics (minimum to maximum %)	PAR (x 10^5 grains cm^{-2} yr^{-1})	Algal communities (minimum to maximum %)	CHAR (particles cm^{-2} yr^{-1})
		(<10 %) and *Abies* (6–23 %) increased. **NAP (4–12 %):** Gradual expansions in Poaceae (<7 %) and *Artemisia* (<3 %).			
5–7 (52.7–51.3 m; 117.0–114.3 ka; 2700 years)	Mixed forest	Peak in *Picea* percentages. **AP (76–95 %):** *Q. robur*-type (7–22 %) and *C. betulus* (3–10 %) values were reduced. *Fagus* was dominant apart from a brief reduction (9–29 %). An abrupt expansion of *Picea* (<11 %) occurred. **NAP (5–24 %):** Further expansions of Poaceae (2–11 %) and *Artemisia* (2–7 %).	Moderate fluctuating PAR (32–144).	Diminished abundances of *P. boryanum* var. *boryanum* (<7 %), *P. boryanum* var. *brevicorne* (<3 %), *Botryococcus* (<7 %) and *T. minimum* (<8 %).	Low fluctuating CHAR (64–788).
5–8 (51.3–49.9 m; 114.3–111.5 ka; 2800 years)	Mixed forest	Re-expansion in *Q. robur*-type and decline in *Fagus*. **AP (65–83 %):** Declines in temperate taxa (42–67 %). *Q. robur*-type expanded to become the dominant taxon (13–29 %) with increases in *Betula* (4–13 %). **NAP (17–35 %):** Increases in Poaceae (6–18 %) and *Artemisia* (4–13 %) values.	Moderate fluctuating PAR (22–162).	Expansion of *P. boryanum* var. *boryanum* (1–32 %) and elevated presence of *P. boryanum* var. *brevicorne* (<4 %).	Low fluctuating CHAR (72–821).
5–9 (49.9–49.5 m; 111.5–110.6 ka; 900 years)	Temperate woodland	Reduced arboreal pollen values and increase in steppe components. **AP (57–71 %):** Reduced abundance of *Q. robur*-type (16–22 %), *Fagus* (3–11 %) and *Betula* (2–13 %). Increasing values of *Pinus* (9–16 %) and *Abies* (6–16 %). **NAP (29–43 %):** Expansion of Poaceae (13–22 %) and *Artemisia* (6–17 %).	Low-moderate increasing PAR (27–67).	Reappearance of *P. kawraiskyi* (2–21 %), reduced population of *P. boryanum* var. *boryanum* (4–10 %), fluctuating expansions of *T. minimum* (0–21 %).	Low fluctuating CHAR (135–532).
5–10 (49.5–48.6 m; 110.6–108.9 ka; 1700 years)	Mixed forest	Recovery of temperate taxa. **AP (62–80 %):** Expansion of *Abies* (7–24 %), *Fagus* (5–16 %) and *C. betulus* (2–10 %). Reduction in *Betula* (3–6 %). **NAP (20–38 %):** Contraction of Poaceae (8–19 %), *Artemisia* (3–11 %) and Amaranthaceae (1–3 %).	Moderate stable PAR (36–91).	Diminished algal community with contraction of *P. kawraiskyi* (0–16 %), *P. boryanum* var. *boryanum* (<8 %), *Botryococcus* (3–9 %) and *T. minimum* (0–15 %).	Low decreasing CHAR (66–630).
5–11 (48.6–48.4 m; 108.9–108.5; 400 years)	Temperate woodland	Reduction in temperate tree values and expansion of steppe taxa. **AP (56–63 %):** Decline in *Abies* (5–8 %), *Fagus* (5–8 %), *C. betulus* (5–9 %) and *Pinus* (8–13 %). *Q. robur*-type increased after an early contraction (15–23 %). **NAP (37–44 %):** Increase in Poaceae (20–22 %) and *Artemisia* (8–14 %) values.	Moderate stable PAR (55–65).	Early expansion of *P. kawraiskyi* (1–8 %). Declining abundance of *P. boryanum* var. *boryanum* (1–4 %) and *T. minimum* (<8 %). Stable presence of *Botryococcus* (4–10 %).	Moderate-high increasing CHAR (969–1466).
5–12 (48.4–47.9 m; 108.5–107.3 ka; 1200 years)	Mixed forest	**AP (59–81 %):** *Q. robur*-type expanded as the dominant taxon (29–41 %). Increases in *Ulmus* (2–7 %), *F. ornus* (<3 %), *Corylus* (<3 %) and *C. betulus* (1–9 %). *Pinus* (4–9 %), *Fagus* (2–7 %) and *Abies* (4–10 %) values declined. **NAP (19–41 %):** Gradual declines in Poaceae (8–20 %) and *Artemisia* (4–10 %).	Moderate fluctuating PAR (28–169).	Diminished algal communities, expansions of *Anabaena* akinetes (<8 %).	Moderate declining CHAR (637–1295).

± 1.0 ka (Table 2; Fig. 6). Following this ~300-year stadial of increased steppe taxa, *Q. robur*-type pollen values substantially increased (30–41 %) along with re-expansions of *Ulmus, Corylus, F. ornus* and *F. excelsior*, indicating warmer, wetter interstadial conditions.

5.2. *Interpreting the $\delta^{18}O$ signal*

Mannella (2020) and Mannella et al. (2019, 2020) showed that most of the carbonate in the F1-F3 boreholes during the interglacial is authigenic (bioinduced) calcite that precipitates during the warmer part of the year (late spring to summer) (Leng and Marshall, 2004). In contrast, glacial samples comprised a larger proportion of minor clastic carbonate and dolomite. The oxygen isotope composition of the authigenic carbonate ($\delta^{18}O_c$) is considered a powerful proxy to reconstruct hydrological changes in the Mediterranean region (Zanchetta et al., 1999, 2022; Roberts et al., 2008; Leng et al., 2010; Dean et al., 2015; Zielhofer et al., 2017). It records the prevailing summer conditions, supporting the reconstruction of changes in the recharge season and the period of summer drought with higher evaporation rates (Li and Ku, 1997; Jones and Roberts, 2008).

Higher $\delta^{18}O_c$ values of lacustrine carbonates during glacial periods are well documented in the Central Mediterranean (Zanchetta et al., 1999, 2007; Roberts et al., 2008), including at the nearby Sulmona Basin (Giaccio et al., 2015), reflecting reduced local precipitation and colder temperatures. The decrease of the $\delta^{18}O_c$ values starting at ~130 ka (Fig. 8) at Fucino indicates a progressive decrease in lake evaporation and increase in precipitation (Zanchetta et al., 2007, 2022; Jones and Roberts, 2008). However, the slow shift in $\delta^{18}O_c$ relative to the rapid expansion of temperate trees at the beginning of the LIG (~129 ka), indicating increasing humidity and temperature, suggests that the hydrological balance of the lake did not respond at the same rate or amplitude to the general climatic amelioration.

The delayed response of the $\delta^{18}O_c$ signal can be explained by the sensitivity of the lake $\delta^{18}O_w$ to summer conditions. The lowest $\delta^{18}O_c$ values occur at ~124.0 ± 1.9 ka, indicating, from a hydrological point of view, the wettest period of the LIG. Before this, summer conditions resulted in greater lake water evaporation and hence still high $\delta^{18}O_c$ values. This is supported by the occurrence of the summer insolation

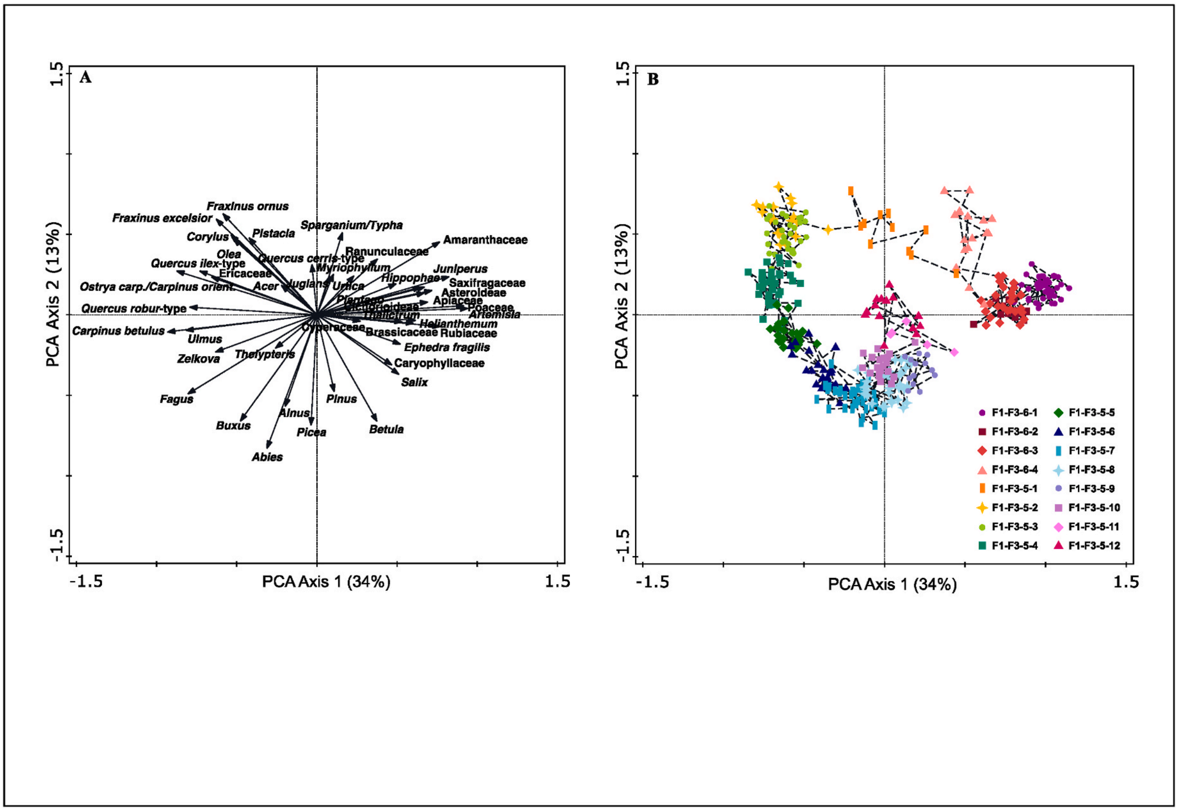

Fig. 7. Principal Component Analysis (PCA) of (a) 45 pollen taxa and (b) 375 samples from core F1-F3 covering the late Penultimate Glacial to early Last Glacial sequence from the Fucino Basin, central Italy. Samples are classified according to the sixteen Pollen Assemblage Zones (PAZs). The labelled axes display the explained variation in species data.

Table 3
Summary output of Principal Component Analysis (PCA) performed on the pollen assemblage of the late Penultimate Glacial to early Last Glacial at Fucino Basin, central Italy.

PCA axes	1	2	3	4
Eigenvalues	0.3394	0.1328	0.0781	0.0466
Explained variation of species data (cumulative)	33.94	47.22	55.03	59.69

Table 4
Spearman's rank correlation coefficients between CHAR and pollen vegetation groups for the entire interval of the late Penultimate Glacial to early Last Glacial and the pollen-based LIG only. Statistically significant correlations (P-value <0.05) are highlighted in bold.

	Late Penultimate Glacial – Last Interglacial – Early Last Glacial	Last Interglacial
Temperate	**0.20**	−0.04
Mediterranean	**0.34**	**0.40**
Pioneer	**−0.43**	**−0.30**
Arboreal	0.07	**−0.23**
Non-arboreal	−0.07	**0.23**
Semi-desert	−0.07	**0.19**

maximum during the first part of the LIG between ~127 and ~129 ka (Fig. 8), highlighting a strong seasonal contrast. Moreover, the appearance and expansion of Mediterranean sclerophylls (*Olea, Phillyrea* and *Pistacia*) at 128.0 ± 1.8 ka indicates increased summer aridity, while the presence of deciduous trees (*Carpinus* and *Fagus*) reflecting substantial winter precipitation. Summer length, drought intensity and biomass are fundamental controls of fires in the Mediterranean (Vannière et al., 2011; Lawson et al., 2013), and the Fucino charcoal accumulation rate tracks NH summer insolation with substantial increases from 130.0 ± 2.0 ka to ~124.4 ± 1.7 ka. Taken together, the palynological and charcoal evidence indicates warmer temperatures, low summer rainfall and increased winter precipitation during the early LIG at Fucino. This is in line with pollen, macrofossil and mineralogical evidence from Tenaghi Philippon, Greece, indicating extreme seasonality of precipitation during the early LIG (Milner et al., 2012).

To explore further the seasonality contrast in the Fucino $\delta^{18}O_c$ record, we can compare it with speleothem $\delta^{18}O_c$ records (Bini et al., 2019). Speleothem $\delta^{18}O_c$ records are less affected by evaporation, being more strictly tied to the amount-weighted average isotopic composition of rainfall during the recharge season, which is mostly the autumn-winter season in central Italy (Drysdale et al., 2004; Zanchetta et al., 2021). The $\delta^{18}O$ signal in speleothems of the central Mediterranean has been attributed to the progressive decrease in the average $\delta^{18}O$ composition of meteoric precipitation linked to the increasing annual/monthly precipitation rate, the so-called "amount effect" (Bard et al., 2002; Natali et al., 2021). Therefore, we can expect that during the period of strong seasonality contrast, lacustrine records dominated by summer evaporation will record higher values and a larger isotopic offset compared to speleothems. The closest speleothem record lies in Antro del Corchia (43°59′N, 10°13′E), a large cave complex in the Alpi Apuane karst of central Italy. It is of similar altitude to Fucino and its recharge system (Piccini et al., 2008), and shows extensive speleothem growth during the LIG (Drysdale et al., 2009; Isola et al., 2019). The stacked $\delta^{18}O$ record was produced by splicing together four stalagmites from the same chamber using the sections with the highest sampling resolution, anchored in time by 87 U/Th dates (Tzedakis et al., 2018). It covers the same time interval as the Fucino record presented here.

Comparison of Fucino $\delta^{18}O$ against the speleothem $\delta^{18}O$ record reveals a substantial negative offset during the transition from the

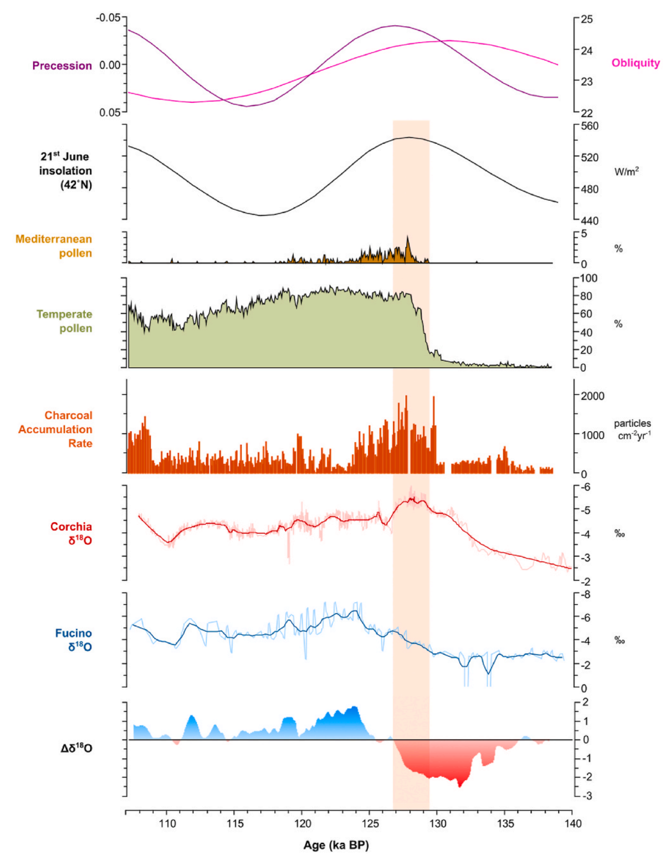

Fig. 8. The difference ($\Delta\delta^{18}O$) between the Fucino Basin bulk carbonate oxygen isotopic composition ($\delta^{18}O$) (‰) and stacked speleothem $\delta^{18}O$ Corchia Cave record (Drysdale et al., 2005; Tzedakis et al., 2018) compared to the Charcoal Accumulation Rate, Temperate and Mediterranean pollen, 21st June insolation at 42°N, precession and obliquity (Laskar et al., 2004). The $\delta^{18}O$ Corchia and Fucino records with rolling averages (bold lines) are plotted. The interval of enhanced seasonality is highlighted in orange.

Penultimate Glacial into the early stages of the LIG (Fig. 8). From 136.0 ± 2.1 ka to 127.0 ± 1.5 ka, there is a large contrast between the two records with $\Delta\delta^{18}O$ values up to 1.8 ‰ lower at Corchia. The ^{18}O-depleted values at Corchia at the end of the Penultimate Glacial reflect the oxygen isotopic composition of seawater at the time of Heinrich 11 (HS11), when meltwater entered the North Atlantic from the collapse of Northern Hemisphere ice sheets during Termination II (Marino et al., 2015; Drysdale et al., 2020). This event altered the isotopic signature of Mediterranean precipitation (Marino et al., 2015). Indeed, applying magnesium (Mg) concentrations from a Corchia Cave speleothem as a palaeotemperature proxy, Drysdale et al. (2020) demonstrated a significant decoupling of Mg and $\delta^{18}O_{speleothem}$ during HS11, with more negative $\delta^{18}O_{speleothem}$ values preceding the Mg-inferred temperature rise. In addition to rainfall amount as the dominant driver, the moisture-source effect evidently plays an important role in determining δ^{18}Ospeleothem during TII. However, the continued large negative offset between 129.5 ± 1.9 ka to ~127 ± 1.5 ka indicates a larger evaporative effect in the Fucino basin. From ~125.0 ± 1.5 ka, a positive offset reflects more negative $\delta^{18}O$ values at Fucino Basin compared to Corchia for the remainder of the LIG and transition into the early Last Glacial. This suggests a reduced seasonal contrast with the evaporative effect at the Fucino basin diminished significantly.

5.3. Wider comparisons

Several long continuous pollen records spanning the LIG period in southern Europe offer scope for regional comparison of the timing and duration of vegetational and environmental changes. However, inherent uncertainties in different dating techniques and age models, as well as variations in archive resolution, complicate comparisons between records. Here, we limit such comparisons to tephrostratigraphically-linked archives from Italy and the Balkans, providing a framework for exploring the spatial and temporal expression of changes during this interval (Regattieri et al., 2014; Zanchetta et al., 2016) ((Fig. 9).

Geographically, one of the closest published LIG palynological records to Fucino is Lago Grande di Monticchio (LGdM) located 280 km to the southeast in Basilicata, southern Italy (Brauer et al., 2007; Allen and Huntley, 2009). Correlation between synchronous vegetation patterns at Fucino and LGdM reveal broadly similar trends through the Penultimate Glacial and LIG (Fig. 10). The LIG onset at LGdM is defined by arboreal vegetation reaching above 50 % at 127.7 ± 6.4 ka (MON14 chronology; Wulf et al., 2012; Martin-Puertas et al., 2014) peaking at 83 % by 127.2 ± 6.4 ka. The 1–2 ka offset compared to Fucino is apparent throughout the LIG and likely a function of variations in sedimentation rates in non-varved sections and the larger uncertainty of the LGdM chronology. During the LIG, Mediterranean pollen percentages were higher at LGdM

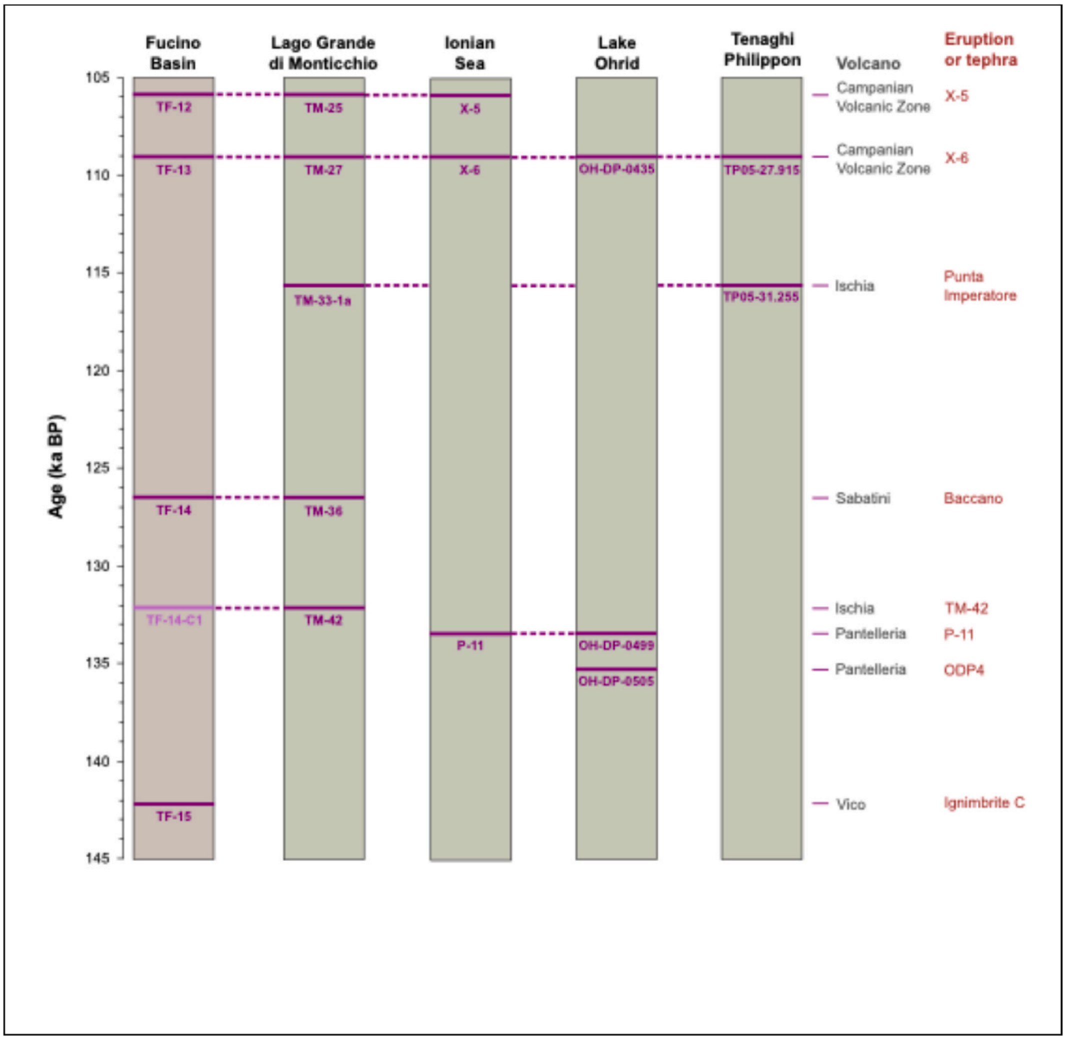

Fig. 9. Tephrostratigraphic framework of selected southern European sites for the period ~145 to 105 ka. Identified and correlated tephra layers with associated volcanic and eruptive source are displayed for the Fucino Basin (Giaccio et al., 2017; Mannella et al., 2019), LGdM (Wulf et al., 2012), Ionian Sea (Keller et al., 1978; Paterne et al., 2008), Lake Ohrid (Leicher et al., 2016) and Tenaghi Philippon (Wulf et al., 2018).

compared to Fucino. This is likely a reflection of a temperature gradient between the two sites with present-day mean annual temperatures of 13.1 °C at LGdM compared to 11.8 °C at Fucino Basin. Spanning an interval of 17.7 ka, LIG conditions at LGdM ended by 109.5 ± 5.4 ka with the opening up of forest vegetation.

The pollen sequence of Lake Ohrid, an extensive lake at the North Macedonia-Albania border displays substantial quantities of *Pinus* and hence high pioneer proportions throughout the late Penultimate Glacial and LIG. The LIG onset at Lake Ohrid is dated to 128.3 ± 2.9 ka (Ohrid modelled age; Leicher et al., 2021) with increases in arboreal percentages beyond 50 %. Similarly, low proportions (up to 3 %) of Mediterranean taxa, as at Fucino, were present in the early LIG. The end of the LIG culminated with a decline in arboreal pollen at ~109.6 ka (Sadori et al., 2016; Sinopoli et al., 2018).

The pollen record from the large fen of Tenaghi Philippon in the Drama Basin, northeast Greece shows a LIG reforestation at 128.7 ± 4.4 ka (TP-2005 chronology; Wulf et al., 2018), with AP values exceeding 50 %. Prior to this, a comparatively drier climate resulted in a glacial landscape heavily dominated by steppe vegetation. The onset of the ensuing Last Glacial at 109.2 ± 1.5 ka, when arboreal taxa drop below 50 % is consistent with Fucino (Milner et al., 2013, 2016).

Of some note is the record of *Fagus* during the LIG. As across much of Europe, *Fagus* presence during the LIG at Lake Ohrid and Tenaghi Philippon appears severely limited or absent, with evidence of presence at LGdM (<10 %). The virtual absence of *Fagus* from most of Europe has been highlighted as a characteristic of the LIG, distinguishing it from other interglacials (Phillips, 1974; Turner, 1975; Tzedakis, 1994). In contrast, the consistently high *Fagus* abundance during the LIG is an exceptional feature of the Fucino pollen record. The taxon persisted continuously from ~128.4 ± 1.8 ka and reached values of 29 % at ~114.6 ± 2.1 ka. This feature likely underlines the importance of the area as a long-term refugium (*sensu* Tzedakis, 1993, 2009) for beech, a reflection of its varied topography and moisture availability providing higher buffering capacity from extreme climate variability.

5.4. Abrupt climate variability

In the following discussion, abrupt climate variability at Fucino during the late Penultimate Glacial to early Last Glacial is explored through comparisons of the temperate tree pollen and charcoal records produced in this research to several other North Atlantic and southern European archives (Fig. 11).

The terminal stadial during the penultimate deglaciation, HS11, is recorded throughout the North Atlantic with associated climatic changes detected globally (Heinrich, 1988; Bond et al., 1992; McManus et al., 1994; Chapman and Shackleton, 1999; Oppo et al., 2001, 2006; Barker et al., 2009, 2011; Barker and Diz, 2014). Within the stadial, three discrete cold events, HS11.1, HS11.2 and HS11.3, interrupted by

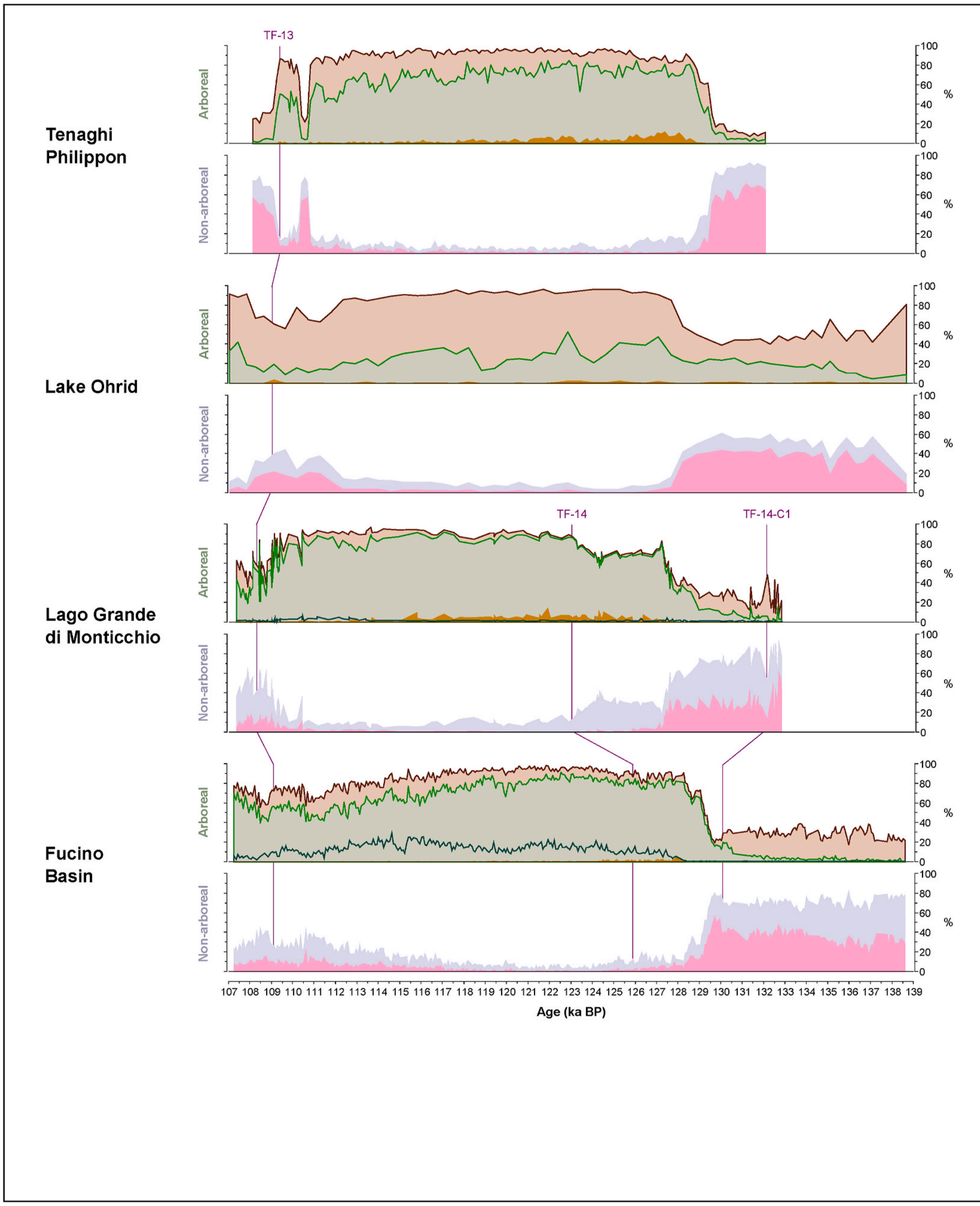

Fig. 10. Comparison of Arboreal (maroon line), Temperate (green line), Pioneer (orange shading), Mediterranean (yellow shading), Fagus (dark green line), Non-arboreal (purple shading) and Semi-desert (pink shading) pollen abundance (%) for the Fucino Basin (this study), Lago Grande di Monticchio (Brauer et al., 2007; Allen and Huntley, 2009), Lake Ohrid (Sadori et al., 2016; Sinopoli et al., 2018) and Tenaghi Philippon (Milner et al., 2013, 2016). Correlative tephras are displayed as labelled purple lines.

warmer conditions have been detected on the Portuguese Margin. Low $\delta^{18}O_{planktonic}$ values during HS11.2 and HS11.3 indicate large meltwater pulses, which in turn would have resulted in surface water stratification, AMOC weakening and associated SST reductions. In parallel, ^{18}O-enriched and ^{13}C-enriched values at Corchia Cave have been related to cooler and drier conditions across the Mediterranean in response to reduced NADW formation (Tzedakis et al., 2018).

At Fucino, one of the most prominent abrupt events during the late Penultimate Glacial occurred at 130.0 ± 2.0 ka to 129.7 ± 2.0 ka (Fig. 12). A contraction in temperate taxa accompanied by elevated charcoal abundance indicates a colder climate with greater aridity, correlative with the final (HS11.3) of three cold events. Comparable signatures of HS11.1 and HS11.2 are not detected in the low abundance refugial tree populations of the late Penultimate Glacial at Fucino. A sudden enrichment in $\delta^{18}O_c$ values at 133.9 ± 2.2 ka, indicating a brief interval of arid conditions, can possibly linked to HS11.1. Subsequent to HS11.1, a transition in algal communities from the dominant *Pediastrum simplex* var. *sturmii* to increasing abundances of *Pediastrum boryanum* var. *brevicorne, Botryococcus* and *Tetraedron minimum* supports the inference of warmer temperatures (Reynolds, 1984; Jankovská and Komárek, 2000; Komárek and Jankovská, 2001; Moss et al., 2003; Ralska-Jasiewiczowa et al., 2003; Niemeyer et al., 2015). Following a peak in the thermophilic taxon *P. boryanum* var. *brevicorne* centred at 133.1 ± 2.1 ka, subsequent expansion in cold-tolerant *Pediastrum kawraiskyi* from 132.7 ± 2.1 ka could reflect cooling associated with HS11.2. This is also detected in the $\delta^{18}O_c$ record as a sudden increase in values centred at 132.3 ± 2.1 ka.

As the Last Interglacial commenced at Fucino, a brief climate

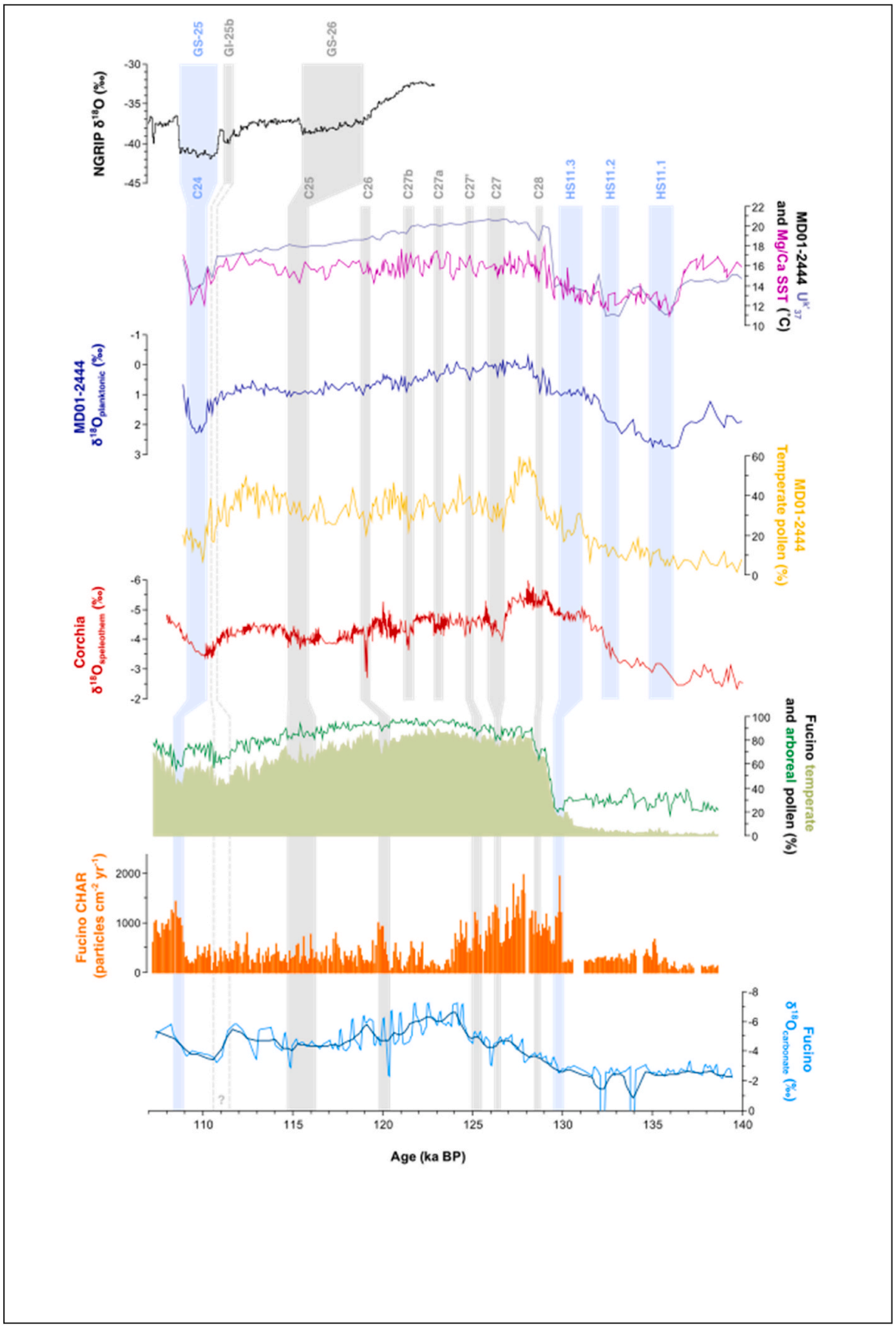

Fig. 11. Comparison of late Penultimate Glacial to early Last Glacial (~140–107 ka) records of NGRIP $\delta^{18}O$ (‰) (NGRIP members, 2004), MD01-2444 alkenone $U^{k'}_{37}$ and Mg/Ca SST (°C), $\delta^{18}O_{planktonic}$ (‰) and temperate tree taxa (%) (Tzedakis et al., 2018), Corchia Cave $\delta^{18}O$ (‰) (Drysdale et al., 2005; Tzedakis et al., 2018), and Fucino temperate and montane taxa (%) and Charcoal Accumulation Rate (CHAR) (particles cm^{-2} yr^{-1}). Abrupt cold events during glacial (light blue) and interglacial (grey) states are highlighted.

reversal to cooler and drier conditions is registered as a decline in temperate tree pollen from 128.8 ± 1.8 ka to 128.4 ± 1.8 ka, correlative with the North Atlantic C28 event at MD01-2444 (Tzedakis et al., 2018) (Figs. 11 and 12). This event occurs prior to a climate amelioration during peak interglacial conditions at 128 ± 1.8 ka characterised by high summer temperatures and enhanced winter precipitation (Milner et al., 2012).

Another decline in temperate tree pollen and increase in CHAR occurs at Fucino from 126.5 ± 1.4 ka to 126.2 ± 1.3 ka. This coincides with the C27 event at ~126.4 ka at MD01-2444, one of the most prominent climatic changes recorded at sites in the North Atlantic (Tzedakis et al., 2018), and linked to meltwaters entering the subpolar North Atlantic (Galaasen et al., 2014) (Figs. 11 and 12). The melting of residual Penultimate Glacial ice masses has been implicated as the driver of instability in NADW ventilation during the early LIG (Galaasen et al., 2014). A climate model experiment using the Earth System Model LOVECLIM under LIG boundary conditions explored the effect of adding 0.05 Sv of freshwater to the northern North Atlantic between ~126.8 and ~126.4 ka, representing event C27 (Tzedakis et al., 2018). The simulated strong cooling over the subpolar North Atlantic produced a deepening of the low-pressure system at mid-to-high latitudes and a strengthening of the subtropical high, leading to strong anticyclonic

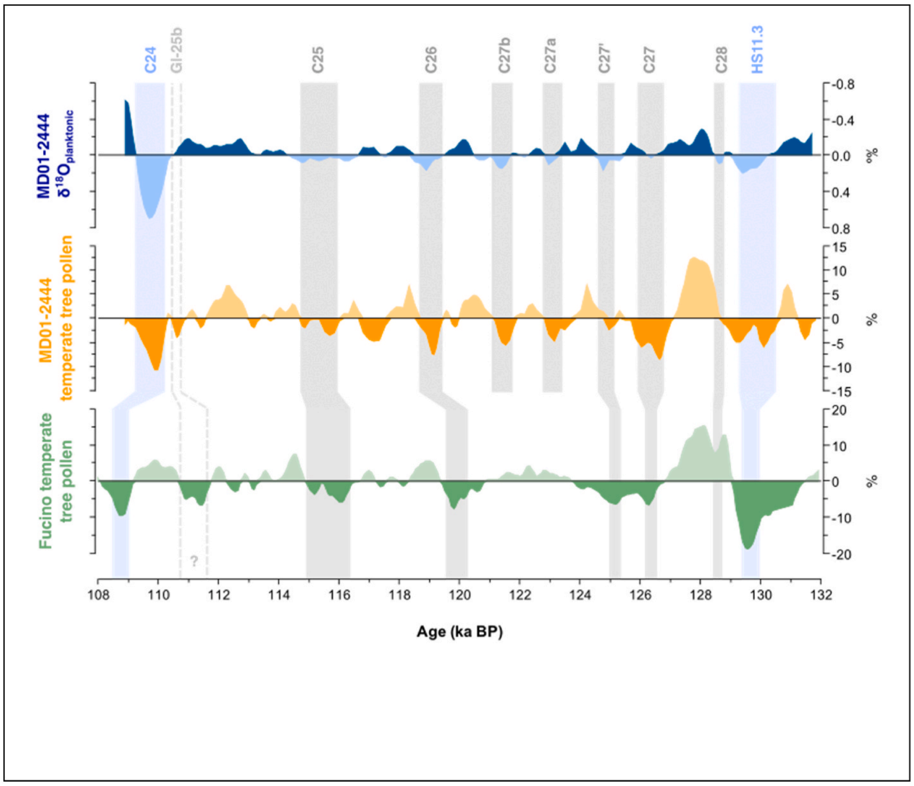

Fig. 12. Comparison of abrupt cold events in Gaussian detrended and smoothed late Penultimate Glacial to early Last Glacial records of Fucino temperate tree pollen (%) against MD01-2444 temperate tree pollen (%) and $\delta^{18}O_{planktonic}$ (‰) (Tzedakis et al., 2018). Abrupt cold events during glacial (light blue) and interglacial (grey) states are highlighted.

circulation over the Mediterranean and drier conditions in southern Europe. The timing of this event is also coherent with a freshwater signal interruption during the deposition of sapropel S5 in the Eastern Mediterranean at 126.5–125.7 ka, implying a reduction in summer monsoon runoff along the North African margin (Amies et al., 2019).

A further cold abrupt event is evident at Fucino from 125.3 ± 1.5 ka to 125.0 ± 1.6 ka (Figs. 11 and 12). The reduction in temperate tree pollen and increased CHAR is a possible expression of the more subdued C27' event recognised in MD01-2444 and Corchia. Two further cold abrupt events appear later in the pollen-based Last Interglacial at Fucino at 120.3 ± 2.1 ka to 119.8 ± 2.2 ka and 116.2 ± 2.1 ka to 114.7 ± 2.1 ka (Figs. 11 and 12), registering as contractions in temperate vegetation with elevated CHAR and $\delta^{18}O_c$-enriched values (Fig. 11). These two events are coeval with the marine cooling events of C26 and C25 at ~119.1 ka and ~117.2 ka, respectively. They are characterised by the widespread decline of North Atlantic surface water temperature and increased ice-rafting activity during a time of Greenland ice regrowth (Adkins et al., 1997; Chapman and Shackleton, 1999; Oppo et al., 2001, 2006; Kopp et al., 2009; Mokeddem et al., 2014; Goelzer et al., 2016). Reduced Mg/Ca SST and enriched $\delta^{18}O_{planktonic}$ values at MD01-2444 are coeval with cold-water mass incursions, whereas a decline in Iberian temperate tree pollen and positive $\delta^{18}O_{speleothem}$ reversals at Corchia reflect the penetration of cool conditions into southern Europe (Tzedakis et al., 2018).

A cold event at 111.5 ± 1.7 ka to 110.9 ± 1.5 ka, possibly corresponding to Greenland Interstadial 25b (GI-25b) (Fig. 11), is recorded as a 17 % decline in temperate tree pollen percentages at Fucino and more positive $\delta^{18}O_c$ values. Comparison against the MD01-2444 record reveals a decline in SST and a positive $\delta^{18}O_{planktonic}$ excursion in addition to a contraction in temperate vegetation and Corchia $\delta^{18}O_{speleothem}$ enrichment centred at ~110.6 ka. Finally, the early Last Glacial commenced at Fucino with a 17 % decline in temperate tree pollen percentages, more positive $\delta^{18}O_c$ values and heightened charcoal deposition over a ~300-year interval. This event correlates with the prominent ice-rafting event C24, coincident with Greenland Stadial 25 (GS25; Fig. 11), and marking the first reactivation of the bipolar seesaw (Capron et al., 2012). It is characterised by prolonged stadial conditions clearly expressed as a distinct drop in North Atlantic SST, significant IRD deposition, a marked shift towards more positive $\delta^{18}O$ values and substantial reductions in temperate trees (Tzedakis et al., 2018).

5.5. The signature of climate variability at Fucino Basin

Atmospheric processes are a possible explanation for the observed LIG variability in the North Atlantic and Europe. Modern day observations and modelling studies have revealed decadal to centennial changes in the North Atlantic subpolar gyre, SST and regional climate in response to an altering strength of the westerly winds associated with the North Atlantic Oscillation (Visbeck et al., 2001; Lohmann et al., 2009). Modelled simulations of the past millennium have additionally demonstrated the role of atmospheric forcing in sea-ice expansion (Drijfhout et al., 2013) and subpolar gyre weakening (Kleppin et al., 2015), with a concomitant shutdown of deep-water formation in the Labrador Sea and centennial-scale AMOC weakening. Alternatively, freshwater input is another potential trigger for AMOC weakening and North Atlantic cooling through increased ocean stratification (Tzedakis et al., 2018). Marine records south of Greenland provide evidence of southern Greenland Ice Sheet retreat and runoff during the LIG (Colville et al., 2011; Hatfield et al., 2016) and document instances of freshwater-induced (Nicholl et al., 2012) reductions in deep-water formation (Galaasen et al., 2014).

Although uncertainties persist regarding the origin and development of abrupt climate variability, the reorganisation of oceanic and atmospheric circulation is key in understanding the close coupling between the North Atlantic and the Mediterranean (Allen et al., 1999; Asioli et al., 1999; Cacho et al., 2001; Rohling et al., 2002; Martrat et al., 2004). North Atlantic cold events have been attributed to a reduction in NADW formation, reduced SSTs and a southward movement of the polar front (Mayewski et al., 1997; Irvalı et al., 2012; Mokeddem et al., 2014).

Despite the high-resolution nature of the Fucino pollen stratigraphy, some abrupt climatic events registered in Greenland, North Atlantic and Mediterranean speleothem records are not captured. For example, no analogous contraction in temperate vegetation occurs during HS11.1, HS11.2, C27a or C27b. One possible explanation is the complexity of ecosystem response to the different external drivers and rates of change associated with each individual abrupt climatic event, which may enact positive or negative feedback loops. Events characterised by a large amplitude of climate change, such as C24, are readily detectable at Fucino and synchronous in vegetation records across Europe (De Beaulieu and Reille, 1984, 1992; Follieri et al., 1989; Watts et al., 1996; Magri and Sadori, 1999; Tzedakis et al., 2003; Brauer et al., 2007; Allen and Huntley, 2009; Milner et al., 2016; Sinopoli et al., 2018; Kern et al., 2022). In these instances, vegetation is responding to an overriding, large-scale abrupt climatic forcing. Vegetation responses to smaller-magnitude events characterised by strong, temporary climate extremes overlaying long-term trends are less consistent. In these cases, site-specific factors including soil moisture availability, physiography, vegetation competition and disturbance may govern internal thresholds in ecological systems producing heterogeneous local changes to a regional climate forcing (Seddon et al., 2015). An ecosystem may thus exhibit stasis under external pressures until a threshold is crossed resulting in an abrupt biotically mediated response (Scheffer et al., 2001; Scheffer and Carpenter, 2003; Folke et al., 2004; Dearing, 2008). In addition, a diversity of microclimates exists within Fucino's large pollen source area and mountainous catchment. Therefore, only climatic stresses of sufficient magnitude would alter vegetation community abundance enough to counteract species range shifts within the rich extent of habitats available (Lawson et al., 2004). Furthermore, the signature of some abrupt events, such as C24 and GI-25b, appears stronger in some Mediterranean long pollen sequences than others. For example, Tenaghi Philippon and LGdM document a more rapid and substantial forest community collapse than Fucino Basin and Lake Ohrid (Brauer et al., 2007; Allen and Huntley, 2009; Milner et al., 2013, 2016). These differences could be explained by variations in moisture availability with precipitation thresholds crossed more readily at Tenaghi Philippon and LGdM prompting a rapid shift to steppe environments, whereas the more humid intermontane locations of Fucino Basin and Lake Ohrid offer a glacial refugium for trees (Koutsodendris et al., 2023).

6. Conclusion

This research has generated a new high-resolution multiproxy record of environmental changes during the late Penultimate Glacial to early Last Glacial at Fucino Basin, central Italy anchored to an independent time-scale, based on high-precision ^{40}Ar/^{39}Ar geochronology, with an uncertainty ranging from ±1.0 ka to 2.2 ka (2σ). It reveals substantial terrestrial and aquatic floristic community turnover in response to changing environmental conditions at Fucino. Comparisons against southern European pollen records reveal regional similarities and a close alignment in glacial-interglacial vegetation succession, but also underline unique site-specific features with respect to vegetative composition, such as the high abundance of *Fagus* throughout the LIG, and the magnitude and timing of climate change responses. A strong hydrological seasonal contrast occurred during the early LIG NH summer insolation maximum (~129–127 ka) with enhanced winter precipitation counteracting high summer aridity. The interval was characterised by more positive $\delta^{18}O_c$ values (compared to the Corchia Cave stalagmite $\delta^{18}O$ record), increased Mediterranean taxa abundance and elevated fire activity. The extreme warmth documented in central Italy during the early LIG appears analogous to future projections of enhanced intensity and frequency of drought and heat stress in the Mediterranean (MedECC, 2020; Lionello et al., 2023). The multiproxy record also documents successive centennial-to millennial-scale climatic events superimposed on glacial-interglacial changes, indicating pronounced changes in temperature and moisture availability. The signature of these abrupt events is documented in palaeoclimatic records from across the North Atlantic realm in which intervals of lowered SSTs in the North Atlantic and Mediterranean Sea are paralleled by reduced forest cover at Fucino. The detection of high-frequency variability at Fucino provides support for a linked North Atlantic and Mediterranean climate regime with North Atlantic cold water mass expansions translating into southern European aridity through atmospheric teleconnections.

CRediT authorship contribution statement

C.A. Roberts: Conceptualization, Methodology, Formal analysis, Visualization, Investigation, Writing – original draft, Writing – review & editing, Project administration, Funding acquisition. **G. Zanchetta:** Conceptualization, Methodology, Investigation, Visualization, Writing – original draft, Writing – review & editing, Funding acquisition. **B. Giaccio:** Conceptualization, Methodology, Investigation, Visualization, Writing – original draft, Writing – review & editing. **S. Nomade:** Investigation, Formal analysis, Visualization, Writing – original draft, Writing – review & editing, Funding acquisition. **G. Mannella:** Investigation, Writing – review & editing. **L. Sadori:** Writing – review & editing. **R. Drysdale:** Writing – review & editing. **M.A. Maslin:** Writing – review & editing. **P.G. Albert:** Investigation, Writing – original draft, Writing – review & editing, Funding acquisition. **C. Smidt:** Investigation. **V.C. Smith:** Writing – review & editing. **M. Flynn:** Investigation. **G. Sottili:** Resources, Writing – review & editing. **B. Wagner:** Investigation, Writing – review & editing. **P.C. Tzedakis:** Conceptualization, Methodology, Writing – original draft, Writing – review & editing, Project administration, Supervision, Funding acquisition.

Declaration of competing interest

The authors declare that they have no known competing financial interests or personal relationships that could have appeared to influence the work reported in this paper.

Acknowledgements

CR was supported through the NERC training grants NE/L002485/1, NE/W502716/1 and NE/S007229/1. PCT acknowledges funding from NERC grant NE/V001620/1. PGA is funded through a UKRI Future Leaders Fellowship (MR/S035478/1). SN received contribution from the CNRS INSU-LEFE for ^{40}Ar/^{39}Ar dating. This article is a contribution of project "FUcino Tephrochronology Unites Quaternary REcords (FUTURE)", supported by the Italian Ministry of Education, University and Research (MIUR, grant PRIN No. 20177TKBXZ_003; G. Zanchetta, coordinator). An international consortium, including IGAG-CNR, IGG-CNR, University of Pisa, INGV-Roma, LIAG-Hannover, University of Cologne, University of Rome La Sapienza, University of Geneva, University of Nottingham, provided the funding for supporting the 2017 Fucino drilling campaign.

Appendix A. Supplementary data

Supplementary data to this article can be found online at https://doi.org/10.1016/j.quascirev.2025.109377.

Data availability

All data and/or code is contained within the submission.

References

Adkins, J.F., Boyle, E.A., Keigwin, L., Cortijo, E., 1997. Variability of the North Atlantic thermohaline circulation during the last interglacial period. Nature 390, 154–156.

Alba-Sánchez, F., López-Sáez, J.A., Pando, B.B., Linares, J.C., Nieto-Lugilde, D., López-Merino, L., 2010. Past and present potential distribution of the Iberian Abies species: a phytogeographic approach using fossil pollen data and species distribution models. Divers. Distrib. 16, 214–228.

Allen, J.R.M., Huntley, B., 2009. Last Interglacial palaeovegetation, palaeoenvironments and chronology: a new record from Lago Grande di Monticchio, southern Italy. Quat. Sci. Rev. 28, 1521–1538.

Allen, J.R.M., Brandt, U., Brauer, A., Hubberten, H.-W., Huntley, B., Keller, J., Kraml, M., Mackensen, A., Mingram, J., Negendank, J.F.W., Nowaczyk, N.R., Oberhänsli, H., Watts, W.A., Wulf, S., Zolitschka, B., 1999. Rapid environmental changes in southern Europe during the last glacial period. Nature 400, 740–743.

Amies, J.D., Rohling, E.J., Grant, K.M., Rodríguez-Sanz, L., Marino, G., 2019. Quantification of african monsoon runoff during last interglacial sapropel S5. Paleoceanogr. Paleoclimatol. 34, 1487–1516.

Asioli, A., Trincardi, F., Lowe, J.J., Oldfield, F., 1999. Short-term climate changes during the Last Glacial–Holocene transition: comparison between Mediterranean records and the GRIP event stratigraphy. J. Quat. Sci. John Wiley Son Ltd 14, 373–381.

Bard, E., Delaygue, G., Rostek, F., Antonioli, F., Silenzi, S., Schrag, D.P., 2002. Hydrological conditions over the western Mediterranean basin during the deposition of the cold Sapropel 6 (ca. 175 kyr BP). Earth Planet Sci. Lett. 202, 481–494.

Barker, S., Diz, P., 2014. Timing of the descent into the last Ice Age determined by the bipolar seesaw. Paleoceanogr. John Wiley Son Ltd 29, 489–507.

Barker, S., Diz, P., Vautravers, M.J., Pike, J., Knorr, G., Hall, I.R., Broecker, W.S., 2009. Interhemispheric Atlantic seesaw response during the last deglaciation. Nature 457, 1097–1102.

Barker, S., Knorr, G., Edwards, R.L., Parrenin, F., Putnam, A.E., Skinner, L.C., Wolff, E., Ziegler, M., 2011. 800,000 Years of abrupt climate variability. Science 334, 347–351.

Bennett, K.D., 2008. Documentation for Psimpoll 4.26 and Pscomp 1.03: C Programs for Plotting Pollen Diagrams and Analysing Pollen Data.

Bennett, K.D., Willis, K.J., 2001. Pollen. In: Smol, J.P., Birks, H.J.B., Last, W.M. (Eds.), Tracking Environmnetal Change Using Lake Sediments: Terrestrial, Algal, and Siliceous Indicators. Kluwer: Springer, Netherlands, pp. 5–32.

Berger, A., Loutre, M.F., 1991. Insolation values for the climate of the last 10 million years. Quat. Sci. Rev. 10, 297–317.

Beug, H.J., 2004. Guide to the Pollen Analysis for Central Europe and the Adjacent Areas, München: Pfeil.

Bini, M., Zanchetta, G., Perşoiu, A., Cartier, R., Català, A., Cacho, I., Dean, J.R., Di Rita, F., Drysdale, R.N., Finnè, M., Isola, I., Jalali, B., Lirer, F., Magri, D., Masi, A., Marks, L., Mercuri, A.M., Peyron, O., Sadori, L., Sicre, M.-A., Welc, F., Zielhofer, C., Brisset, E., 2019. The 4.2kaBP Event in the Mediterranean region: an overview. Clim. Past 15, 555–577.

Birks, H.J.B., Birks, H.H., 1980. Quaternary Palaeoecology. Edward Arnold, London.

Blaauw, M., Christen, J.A., 2011. Flexible paleoclimate age-depth models using an autoregressive gamma process. Bayesian Anal. Int. Soc. Bayesian Anal. 6, 457–474.

Blasi, C., Di Pietro, R., Fortini, P., Catonica, C., 2003. The main plant community types of the alpine belt of the Apennine chain. Plant Biosyst. Taylor Francis 137, 83–110.

Blasi, C., Capotorti, G., Copiz, R., Guida, D., Mollo, B., Smiraglia, D., Zavattero, L., 2014. Classification and mapping of the ecoregions of Italy. Plant Biosyst. Taylor Francis 148, 1255–1345.

Blasi, C., Capotorti, G., Copiz, R., Guida, D., Barbara, M., Smiraglia, D., Zavattero, L., 2018. Terrestrial Ecoregions of Italy: Sections and Subsections. University of Rome 'Sapienza'.

Blockley, S.P.E., Pyne-O'Donnell, S.D.F., Lowe, J.J., Matthews, I.P., Stone, A., Pollard, A.M., Turney, C.S.M., Molyneux, E.G., 2005. A new and less destructive laboratory procedure for the physical separation of distal glass tephra shards from sediments. Quat. Sci. Rev. 24, 1952–1960.

Bolker, B., Warnes, G.R., Lumley, T., 2022. gtools. Github. Available at: https://github.com/r-gregmisc/gtools.

Bond, G., Heinrich, H., Broecker, W., Labeyrie, L., McManus, J., Andrews, J., Huon, S., Jantschik, R., Clasen, S., Simet, C., Tedesco, K., Klas, M., Bonani, G., Ivy, S., 1992. Evidence for massive discharges of icebergs into the North Atlantic ocean during the last glacial period. Nature 360, 245–249.

Branca, S., Cinquegrani, A., Cioni, R., Conte, A.M., Conticelli, S., De Astis, G., de Vita, S., Rosa, R., Di Vito, M.A., Donato, P., Forni, F., Francalanci, L., Gaeta, M., Giaccio, B., Giordano, G., Giuffrida, M., Isaia, R., Lucchi, F., Marra, F., Viccaro, M., 2023. The Italian Quaternary volcanism. Alp. Mediterr. Quat. 36, 221–284.

Brauer, A., Allen, J.R.M., Mingram, J., Dulski, P., Wulf, S., Huntley, B., 2007. Evidence for last interglacial chronology and environmental change from Southern Europe. Proc. Natl. Acad. Sci. 104, 450–455.

Burri, E., Petitta, M., 1998. Groundwater drawdown in karstic aquifers due to agricultural activity in the Fucino Plain (Abruzzi, central Italy). Acta Carsologica 27, 27–46.

Burri, E., Petitta, M., 2004. Agricultural changes affecting water availability: from abundance to scarcity (Fucino Plain, central Italy). Irrig. Drain. John Wiley Son Ltd 53, 287–299.

Cacho, I., Grimalt, J.O., Canals, M., Sbaffi, L., Shackleton, N.J., Schönfeld, J., Zahn, R., 2001. Variability of the western Mediterranean Sea surface temperature during the last 25,000 years and its connection with the Northern Hemisphere climatic changes. Paleoceanogr. John Wiley Son Ltd 16, 40–52.

Camuera, J., Jiménez-Moreno, G., Ramos-Román, M.J., García-Alix, A., Toney, J.L., Anderson, R.S., Jiménez-Espejo, F., Kaufman, D., Bright, J., Webster, C., Yanes, Y., Carrión, J.S., Ohkouchi, N., Suga, H., Yamame, M., Yokoyama, Y., Martínez-Ruiz, F., 2018. Orbital-scale environmental and climatic changes recorded in a new ∼200,000-year-long multiproxy sedimentary record from Padul, southern Iberian Peninsula. Quat. Sci. Rev. 198, 91–114.

Camuera, J., Jiménez-Moreno, G., Ramos-Román, M.J., García-Alix, A., Toney, J.L., Anderson, R.S., Jiménez-Espejo, F., Bright, J., Webster, C., Yanes, Y., Carrión, J.S., 2019. Vegetation and climate changes during the last two glacial-interglacial cycles in the western Mediterranean: a new long pollen record from Padul (southern Iberian Peninsula). Quat. Sci. Rev. 205, 86–105.

CAPE, 2006. Last Interglacial Arctic warmth confirms polar amplification of climate change. Quat. Sci. Rev. 25, 1383–1400.

Capron, E., Landais, A., Chappellaz, J., Buiron, D., Fischer, H., Johnsen, S.J., Jouzel, J., Leuenberger, M., Masson-Delmotte, V., Stocker, T.F., 2012. A global picture of the first abrupt climatic event occurring during the last glacial inception. Geophys. Res. Lett. John. Wiley Son Ltd 39, 1–8.

Capron, E., Govin, A., Stone, E.J., Masson-Delmotte, V., Mulitza, S., Otto-Bliesner, B., Rasmussen, T.L., Sime, L.C., Waelbroeck, C., Wolff, E.W., 2014. Temporal and spatial structure of multi-millennial temperature changes at high latitudes during the Last Interglacial. Quat. Sci. Rev. 103, 116–133.

Cara, F., Di Giulio, G., Cavinato, G.P., Famiani, D., Milana, G., 2011. Seismic characterization and monitoring of Fucino Basin (Central Italy). Bull. Earthq. Eng. 9, 1961–1985.

Cavinato, G.P., Carusi, C., Dall'Asta, M., Miccadei, E., Piacentini, T., 2002. Sedimentary and tectonic evolution of Plio–Pleistocene alluvial and lacustrine deposits of Fucino Basin (central Italy). Lacustrine Depos. Syst. 148, 29–59.

Chapman, M.R., Shackleton, N.J., 1999. Global ice-volume fluctuations, North Atlantic ice-rafting events, and deep-ocean circulation changes between 130 and 70 ka. Geology 27, 795–798.

Clark, J.S., 1988. Particle motion and the ignificance of the green alga Botryococcus in the lacustrine rotliegend (upper carboniferous - lower permian). Hist. Biol. Taylor Francis 13, 221–234.

Clausing, A., 1999. Palaeoenvironmental significance of the green alga Botryococcus in the lacustrine rotliegend (upper carboniferous - lower permian). Hist. Biol. 13, 221–234.

Climate Data, 2023. Avezzano climate (Italy). https://en.climate-data.org/europe/italy/abruzzo/avezzano-14382/#climate-graph (accessed March 2023).

Colville, E.J., Carlson, A.E., Beard, B.L., Hatfield, R.G., Stoner, J.S., Reyes, A.V., Ullman, D.J., 2011. 'Sr-Nd-Pb isotope evidence for ice-sheet presence on southern Greenland during the last interglacial', *science*. Am. Assoc. Adv. Sci. 333, 620–623.

Conti, F., Bartolucci, F., 2015. The Vascular Flora of the National Park of Abruzzo, Lazio and Molise (Central Italy): an Annotated Checklist. Springer, London.

Conti, F., Abbate, G., Alessandrini, A., Blasi, C., 2005. An Annotated Checklist of the Italian Vascular Flora. Palombi Editori, Rome.

Cushing, E.J., 1967. Evidence for differential pollen preservation in late quaternary sediments in Minnesota. Rev. Palaeobot. Palynol. 4, 87–101.

De Beaulieu, J.L., Reille, M., 1984. 'A long upper Pleistocene pollen record from Les Echets, near Lyon, France', Boreas, 13. John Wiley & Sons, Ltd, pp. 111–132.

De Beaulieu, J.-L., Reille, M., 1992. Long Pleistocene pollen sequences from the Velay plateau (massif central, France). Veg. Hist. Archaeobotany 1, 233–242.

De Sillo, R., Sanctis, M., Bruno, F., Attorre, F., 2012. Vegetation and landscape of the Simbruini mountains (central Apennines). Plant Sociol. 49, 3–64.

Dean, J.R., Jones, M.D., Leng, M.J., Noble, S.R., Metcalfe, S.E., Sloane, H.J., Sahy, D., Eastwood, W.J., Roberts, C.N., 2015. Eastern Mediterranean hydroclimate over the late glacial and Holocene, reconstructed from the sediments of Nar lake, central Turkey, using stable isotopes and carbonate mineralogy. Quat. Sci. Rev. 124, 162–174.

Dearing, J.A., 2008. Landscape change and resilience theory: a palaeoenvironmental assessment from Yunnan, SW China. Holocene SAGE Publ. Ltd. 18, 117–127.

Di Roberto, A., Smedile, A., Del Carlo, P., De Martini, P.M., Iorio, M., Petrelli, M., Pantosti, D., Pinzi, S., Todrani, A., 2018. Tephra and cryptotephra in a ∼ 60,000-year-old lacustrine sequence from the Fucino Basin: new insights into the major explosive events in Italy. Bull. Volcanol. 80, 1–23.

Drijfhout, S., Gleeson, E., Dijkstra, H.A., Livina, V., 2013. Spontaneous abrupt climate change due to an atmospheric blocking–sea-ice–ocean feedback in an unforced climate model simulation. Proc. Nat. Acad. Sci. 110, 19713–19718.

Drysdale, R.N., Zanchetta, G., Hellstrom, J.C., Fallick, A.E., Zhao, J., 2005. Stalagmite evidence for the onset of the Last Interglacial in southern Europe at 129 ± 1. Geophys. Res. Lett. 32, 1–4. John Wiley & Sons, Ltd.

Drysdale, R.N., Zanchetta, G., Hellstrom, J.C., Fallick, A.E., Zhao, J., Isola, I., Bruschi, G., 2004. Palaeoclimatic implications of the growth history and stable isotope (δ18O and δ13C) geochemistry of a Middle to Late Pleistocene stalagmite from central-western Italy. Earth Planet Sci. Lett. 227, 215–229.

Drysdale, R.N., Hellstrom, J.C., Zanchetta, G., Fallick, A.E., Sánchez Goñi, M.F., Couchoud, I., McDonald, J., Maas, R., Lohmann, G., Isola, I., 2009. Evidence for obliquity forcing of glacial termination II. Science 325, 1527–1531.

Drysdale, R., Couchoud, I., Zanchetta, G., Isola, I., Regattieri, E., Hellstrom, J., Govin, A., Tzedakis, P.C., Ireland, T., Corrick, E., Greig, A., Wong, H., Piccini, L., Holden, P., Woodhead, J., 2020. Magnesium in subaqueous speleothems as a potential palaeotemperature proxy. Nat. Commun. 11, 1–11.

Elliott, J.A., Jones, I.D., Thackeray, S.J., 2006. Testing the sensitivity of phytoplankton communities to changes in water temperature and nutrient Load, in a temperate lake. Hydrobiologia 559, 401–411.

Fægri, K., Iversen, J., 1989. Textbook of Pollen Analysis, fourth ed. John Wiley and Sons, Chichester.

Fairbridge, R.W., 1972. Climatology of a glacial cycle. Quat. Res. 2, 283–302.

Falcone, R., Falgiani, A., Parisse, B., Petitta, M., Spizzico, M., Tallini, M., 2008. Chemical and isotopic (δ18O‰, δ2H‰, δ13C‰, 222Rn) multi-tracing for groundwater conceptual model of carbonate aquifer (Gran Sasso INFN underground laboratory – central Italy). J. Hydrol. 357, 368–388.
Fernandez, G., Giaccio, B., Costa, A., Monaco, L., Nomade, S., Albert, P.G., Pereira, A., Flynn, M., Leicher, N., Lucchi, F., Petrosino, P., Palladino, D.M., Milia, A., Insinga, D. D., Wulf, S., Kearney, R., Veres, D., Jordanova, D., Putignano, M.L., Isaia, R., Sottili, G., 2024. New constraints on the Middle-Late Pleistocene Campi Flegrei explosive activity and Mediterranean tephrostratigraphy (~160 ka and 110–90 ka). Quat. Sci. Rev. 331.
Filibeck, G., Cancellieri, L., Sperandii, M.G., Belonovskaya, E., Sobolev, N., Tsarevskaya, N., Becker, T., Berastegi, A., Bückle, C., Che, R., Conti, F., Dembicz, I., Fantinato, E., Frank, D., Frattaroli, A.R., García-Mijangos, I., Guglielmino, A., Janišová, M., Maestri, S., Biurrun, I., 2018. Biodiversity patterns of dry grasslands in the Central Apennines (Italy) along a precipitation gradient: experiences and first results from the 10th EDGG Field Workshop. Bullrt. Eur. Gry Grassland Group 36, 25–41.
Filibeck, G., Cancellieri, L., Bartolucci, F., Becker, U., Conti, F., Maestri, S., Mürz, M., Schommer, E., Sperandii, M.G., Becker, T., 2019. Festuca valesiaca Schleich. ex Gaudin newly discovered in the Central Apennines (Italy): a further example of steppe relict in the Abruzzo "dry valleys". Plant Biosyst. 154, 1–8.
Finsinger, W., Tinner, W., 2005. Minimum count sums for charcoal concentration estimates in pollen slides: accuracy and potential errors. Holocene SAGE Publ. Ltd. 15, 293–297.
Fischer, H., Meissner, K.J., Mix, A.C., Abram, N.J., Austermann, J., Brovkin, V., Capron, E., Colombaroli, D., Daniau, A.-L., Dyez, K.A., Felis, T., Finkelstein, S.A., Jaccard, S.L., McClymont, E.L., Rovere, A., Sutter, J., Wolff, E.W., Affolter, S., Bakker, P., Ballesteros-Cánovas, J.A., Barbante, C., Caley, T., Carlson, A.E., Churakova (Sidorova), O., Cortese, G., Cumming, B.F., Davis, B.A.S., de Vernal, A., Emile-Geay, J., Fritz, S.C., Gierz, P., Gottschalk, J., Holloway, M.D., Joos, F., Kucera, M., Loutre, M.-F., Lunt, D.J., Marcisz, K., Marlon, J.R., Martinez, P., Masson-Delmotte, V., Nehrbass-Ahles, C., Otto-Bliesner, B.L., Raible, C.C., Risebrobakken, B., Sánchez Goñi, M.F., Arrigo, J.S., Sarnthein, M., Sjolte, J., Stocker, T.F., Velasquez Alvárez, P.A., Tinner, W., Valdes, P.J., Vogel, H., Wanner, H., Yan, Q., Yu, Z., Ziegler, M., Zhou, L., 2018. Palaeoclimate constraints on the impact of 2 °C anthropogenic warming and beyond. Nat. Geosci. 11, 474–485.
Florschütz, F., Menéndez Amor, J., Wijmstra, T.A., 1971. Palynology of a thick quaternary succession in southern Spain. Palaeogeogr. Palaeoclimatol. Palaeoecol. 10, 233–264.
Folke, C., Carpenter, S., Walker, B., Scheffer, M., Elmqvist, T., Gunderson, L., Holling, C. S., 2004. 'Regime shifts, resilience, and biodiversity in ecosystem Management', *annual Review of ecology, evolution, and systematics*. Annu.Rev. 35, 557–581.
Follieri, M., Magri, D., Sadori, L., 1988. 250,000-year pollen record from Valle di Castiglione (Roma). Pollen Spores 3–4, 329–356.
Follieri, M., Magri, D., Sadori, L., 1989. Pollen stratigraphical synthesis from Valle di Castiglione (Roma). Quat. Int. 3/4, 81–84.
Galaasen, E.V., Ninnemann, U.S., Irvalı, N., Kleiven, H., Kikki, F., Rosenthal, Y., Kissel, C., Hodell, D.A., 2014. Rapid reductions in North Atlantic deep water during the peak of the last interglacial period. Science 343, 1129–1132.
Galadini, F., Messina, P., 2004. Early–Middle Pleistocene eastward migration of the Abruzzi Apennine (central Italy) extensional domain. J. Geodyn. 37, 57–81.
Galli, P., Giaccio, B., Messina, P., Peronace, E., 2016. Three magnitude 7 earthquakes on a single fault in central Italy in 1400 years, evidenced by new palaeoseismic results. Terra Nova 28, 146–154.
Ganopolski, A., Robinson, A., 2011. The past is not the future. Nat. Geosci. 4, 661–663.
Giaccio, B., Nomade, S., Wulf, S., Isaia, R., Sottili, G., Cavuoto, G., Galli, P., Messina, P., Sposato, A., Sulpizio, R., Zanchetta, G., 2012. The late MIS 5 Mediterranean tephra markers: a reappraisal from peninsular Italy terrestrial records. Quat. Sci. Rev. 56, 31–45.
Giaccio, B., Regattieri, E., Zanchetta, G., Wagner, B., Galli, P., Mannella, G., Niespolo, E., Peronace, E., Renne, P.R., Nomade, S., Cavinato, G.P., Messina, P., Sposato, A., Boschi, C., Florindo, F., Marra, F., Sadori, L., 2015. A key continental archive for the last 2 Ma of climatic history of the central Mediterranean region: a pilot drilling in the Fucino Basin, central Italy. Sci. Drill. 20, 13–19.
Giaccio, B., Niespolo, E.M., Pereira, A., Nomade, S., Renne, P.R., Albert, P.G., Arienzo, I., Regattieri, E., Wagner, B., Zanchetta, G., Gaeta, M., Galli, P., Mannella, G., Peronace, E., Sottili, G., Florindo, F., Leicher, N., Marra, F., Tomlinson, E.L., 2017. First integrated tephrochronological record for the last ~190 kyr from the Fucino Quaternary lacustrine succession, central Italy. Quat. Sci. Rev. 158, 211–234.
Giaccio, B., Leicher, N., Mannella, G., Monaco, L., Regattieri, E., Wagner, B., Zanchetta, G., Gaeta, M., Marra, F., Nomade, S., Palladino, D.M., Pereira, A., Scheidt, S., Sottili, G., Wonik, T., Wulf, S., Zeeden, C., Ariztegui, D., Cavinato, G.P., Dean, J.R., Florindo, F., Leng, M.J., Macrì, P., Niespolo, E., Renne, P.R., Rolf, C., Sadori, L., Thomas, C., Tzedakis, P.C., 2019. Extending the tephra and palaeoenvironmental record of the Central Mediterranean back to 430 ka: a new core from Fucino Basin, central Italy. Quat. Sci. Rev. 225, 1–21.
Giesecke, T., Bennett, K.D., 2004. The Holocene spread of Picea abies (L.) Karst. in Fennoscandia and adjacent areas. J Biogeogr. 31, 1523–1548.
Giraudi, C., 1989. Lake levels and climate for the last 30,000 years in the Fucino area (Abruzzo-Central Italy) — a review. Palaeogeogr. Palaeoclimatol. Palaeoecol. 70, 249–260.
Giraudi, C., 1998. Late Pleistocene and Holocene lake-level variations in Fucino Lake (Abruzzo, central Italy) inferred from geological, archaeological and historical data. Palaeoclim. Res. 25, 1–17.
Giraudi, C., 2002. 'The Variations of the Calderone Glacier (Gran Sasso d'Italia, Abruzzo, Central Italy) and the Climatic Oscillations during the Last 3000 Years, vol. 15, pp. 149–154.
Giraudi, C., Frezzotti, M., 1997. Late Pleistocene glacial events in the central Apennines, Italy. Quat. Res. 48, 280–290.
Giaccio, B., Wagner, B., Zanchetta, G., Bertini, A., Cavinato, G.P., de Franco, R., Florindo, F., Hodell, D.A., Neubauer, T.A., Nomade, S., Pereira, A., Sadori, L., Satolli, S., Tzedakis, P.C., Albert, P., Boncio, P., De Jonge, C., Francke, A., Heim, C., Masi, A., Marchegiano, M., Roberts, H.M., Noren, A., & team, the M., 2024. International Continental Scientific Drilling Program (ICDP) workshop on the Fucino paleolake project: the longest continuous terrestrial archive in the MEditerranean recording the last 5 Million years of Earth system history (MEME). Sci. Drill. 33, 249–266.
Giraudi, C., Giaccio, B., 2015. Middle Pleistocene Glaciations in the Apennines, Italy: New Chronological Data and Preservation of the Glacial Record, vol. 433. Geological Society, London, Special Publications, pp. 161–178.
Goelzer, H., Huybrechts, P., Loutre, M.-F., Fichefet, T., 2016. Last Interglacial climate and sea-level evolution from a coupled ice sheet–climate model. Clim. Past 12, 2195–2213.
Gulev, S.K., Thorne, P.W., Ahn, J., Dentener, F.J., Domingues, C.M., Gerland, S., Gong, D., Kaufman, D.S., Nnamchi, H.C., Quaas, J., Rivera, J.A., Sathyendranath, S., Smith, S.L., Trewin, B., von Schuckmann, K., Vose, R.S., 2021. Changing state of the climate system. In: Masson-Delmotte, V., Zhai, P., Pirani, A., Connors, S.L., Péan, C., Berger, S., Caud, N., Chen, Y., Goldfarb, L., Gomis, M.I., Huang, M., Leitzell, K., Lonnoy, E., Matthews, J.B.R., Maycock, T.K., Waterfield, T., Yelekçi, O., Yu, R., Zhou, B. (Eds.), Climate Change 2021: the Physical Science Basis. Contribution of Working Group I to the Sixth Assessment Report of the Intergovernmental Panel on Climate Change. Cambridge University Press, Cambridge, UK, pp. 287–422.
Guy-Ohlson, D., 1992. Botryococcus as an aid in the interpretation of palaeoenvironment and depositional processes. Rev. Palaeobot. Palynol. 71, 1–15.
Hatfield, R.G., Reyes, A.V., Stoner, J.S., Carlson, A.E., Beard, B.L., Winsor, K., Welke, B., 2016. Interglacial responses of the southern Greenland ice sheet over the last 430,000 years determined using particle-size specific magnetic and isotopic tracers. Earth Planet Sci. Lett. 454, 225–236.
Heinrich, H., 1988. Origin and consequences of cyclic ice rafting in the Northeast Atlantic Ocean during the past 130,000 years. Quat. Res. 29, 142–152.
Hillbrand, M., van Geel, B., Hasenfratz, A., Hadorn, P., Haas, J.N., 2014. Non-pollen palynomorphs show human- and livestock-induced eutrophication of Lake Nussbaumersee (Thurgau, Switzerland) since Neolithic times (3840 BC). Holocene SAGE Publ. Ltd. 24, 559–568.
Hoffman, J.S., Clark, P.U., Parnell, A.C., He, F., 2017. Regional and global sea-surface temperatures during the last interglaciation. Science 355, 276–279.
Huntley, B., Birks, H.J.B., 1983. An Atlas of Past and Present Pollen Maps for Europe: 0-13000 Years Ago. Cambridge University Press, Cambridge.
Irvalı, N., Ninnemann, U.S., Galaasen, E.V., Rosenthal, Y., Kroon, D., Oppo, D.W., Kleiven, H.F., Darling, K.F., Kissel, C., 2012. Rapid switches in subpolar North Atlantic hydrography and climate during the Last Interglacial (MIS 5e). Paleoceanogr. John Wiley Son Ltd 27, 1–16.
Isola, I., Ribolini, A., Zanchetta, G., Bini, M., Regattieri, E., Drysdale, R.N., Hellstrom, J. C., Bajo, P., Montagna, P., Pons-Branchu, E., 2019. Speleothem U/Th age constraints for the last glacial conditions in the Apuan Alps, northwestern Italy. Palaeogeogr. Palaeoclimatol. Palaeoecol. 518, 62–71.
Jankovská, V., Komárek, J., 2000. Indicative value of Pediastrum and other coccal green algae in palaeoecology. Folia Geobot. 35, 59–82.
Jones, M.D., Roberts, N.C., 2008. Interpreting lake isotope records of Holocene environmental change in the Eastern Mediterranean. Last 15ka Environ. Change Meditter, Reg. Inter. Diff. Arch. 181, 32–38.
Juggins, S., 2007. C2 Version 1.5 User Guide: Software for Ecological and Palaeoecological Data Analysis and Visualisation. Newcastle University, Newcastle upon Tyne, p. 73.
Keller, J., Ryan, W.B.F., Ninkovich, D., Altherr, R., 1978. Explosive volcanic activity in the Mediterranean over the past 200,000 yr as recorded in deep-sea sediments. GSA Bull. 89, 591–604.
Kern, O.A., Koutsodendris, A., Allstädt, F.J., Mächtle, B., Peteet, D.M., Kalaitzidis, S., Christanis, K., Pross, J., 2022. A near-continuous record of climate and ecosystem variability in Central Europe during the past 130 kyrs (Marine Isotope Stages 5–1) from Füramoos, southern Germany. Quat. Sci. Rev. 284, 1–19.
Kleppin, H., Jochum, M., Otto-Bliesner, B., Shields, C.A., Yeager, S., 2015. Stochastic atmospheric forcing as a cause of Greenland climate transitions. J. Clim. Boston MA USA: Am. Meterorol. Soc. 28, 7741–7763.
Komárek, J., Jankovská, V., 2001. Review of the Green Algal Genus Pediastrum; Implication for Pollen-Analytical Research. Schweizerbart Science Publishers, Stuttgart, Germany.
Kopp, R.E., Simons, F.J., Mitrovica, J.X., Maloof, A.C., Oppenheimer, M., 2009. Probabilistic assessment of sea level during the last interglacial stage. Nature 462, 863–867.
Köppen, W., 1918. Klassification der Klimate nach Temperatur, Niederschlag and Jahreslauf. Petermanns Geogr. Mitt. 64, 193–203.
Koutsodendris, A., Dakos, V., Fletcher, W.J., Knipping, M., Kotthoff, U., Milner, A.M., Müller, U.C., Kaboth-Bahr, S., Kern, O.A., Kolb, L., Vakhrameeva, P., Wulf, S., Christanis, K., Schmiedl, G., Pross, J., 2023. Atmospheric CO2 forcing on Mediterranean biomes during the past 500 kyrs. Nat. Commun. 14, 1–12.
Krawchuk, M.A., Moritz, M.A., 2011. Constraints on global fire activity vary across a resource gradient. Ecol. 92, 121–132.
Kühl, N., Litt, T., 2003. Quantitative time series reconstruction of Eemian temperature at three European sites using pollen data. Veg. Hist. Archaeobotany 12, 205–214.

Kukla, G.J., Bender, M.L., de Beaulieu, J.-L., Bond, G., Broecker, W.S., Cleveringa, P., Gavin, J.E., Herbert, T.D., Imbrie, J., Jouzel, J., Keigwin, L.D., Knudsen, K.-L., McManus, J.F., Merkt, J., Muhs, D.R., Müller, H., Poore, R.Z., Porter, S.C., Seret, G., Shackleton, N.J., Turner, C., Tzedakis, P.C., Winograd, I.J., 2002. Last interglacial climates. Quat. Res. 58, 2–13.

Lang, N., Wolff, E.W., 2011. Interglacial and glacial variability from the last 800 ka in marine, ice and terrestrial archives. Clim. Past 7, 361–380.

Laskar, J., Robutel, P., Joutel, F., Gastineau, M., Correia, A.C.M., Levrard, B., 2004. A long-term numerical solution for the insolation quantities of the Earth. Astron. Astrophys. 428, 261–285.

Laurenzi, M.A., Villa, I.M., 1987. 40Ar/39Ar chronostratigraphy of Vico ignimbrites. Period. Mineral. 56, 285–293.

Lawson, I., Frogley, M., Bryant, C., Preece, R., Tzedakis, P., 2004. The Lateglacial and Holocene environmental history of the Ioannina basin, north-west Greece. Quat. Sci. Rev. 23, 1599–1625.

Lawson, I.T., Tzedakis, P.C., Roucoux, K.H., Galanidou, N., 2013. The anthropogenic influence on wildfire regimes: charcoal records from the Holocene and Last Interglacial at Ioannina, Greece. J. Biogeogr. 40, 2324–2334.

Leicher, N., Giaccio, B., Zanchetta, G., Sulpizio, R., Albert, P.G., Tomlinson, E.L., Lagos, M., Francke, A., Wagner, B., 2021. Lake Ohrid's tephrochronological dataset reveals 1.36 Ma of Mediterranean explosive volcanic activity. Sci. Data 8, 231.

Leicher, N., Giaccio, B., Pereira, A., Nomade, S., Monaco, L., Mannella, G., Galli, P., Peronance, E., Palladino, D.M., Sottili, G., Zanchetta, G., Wagner, B., 2023. Central Mediterranean tephrochronology between 313 and 366 ka: new insights from the Fucino palaeolake sediment succession. Boreas 52, 240–271.

Leng, M.J., Marshall, J.D., 2004. Palaeoclimate interpretation of stable isotope data from lake sediment archives. Isot. Quat. Paleoenviron. Reconstr. 23, 811–831.

Leicher, N., Zanchetta, G., Sulpizio, R., Giaccio, B., Wagner, B., Nomade, S., Francke, A., Del Carlo, P., 2016. First tephrostratigraphic results of the DEEP site record from Lake Ohrid (Macedonia and Albania). Biogeosciences 13, 2151–2178.

Leng, M.J., Jones, M.D., Frogley, M.R., Eastwood, W.J., Kendrick, C.P., Roberts, C.N., 2010. Detrital carbonate influences on bulk oxygen and carbon isotope composition of lacustrine sediments from the Mediterranean. Oxyg. Isot. Traces Mediterr. Var. : Link. Past Present Future 71, 175–182.

Li, H.C., Ku, T.L., 1997. δ13C–δ18C covariance as a paleohydrological indicator for closed-basin lakes. Palaeogeogr. Palaeoclimatol. Palaeoecol. 133, 69–80.

Lionello, P., Malanotte-Rizzoli, P., Boscolo, R. (Eds.), 2006. Mediterranean Climate Variability. Elsevier, London (Developments in Earth and Environmental Sciences).

Lionello, P., Giorgi, F., Rohling, E., Seager, R., 2023. Chapter 3 - mediterranean climate: past, present and future. In: Schroeder, K., Chiggiato, J. (Eds.), Oceanography of the Mediterranean Sea. Elsevier, pp. 41–91.

Lohmann, K., Drange, H., Bentsen, M., 2009. Response of the North Atlantic subpolar gyre to persistent North Atlantic oscillation like forcing. Clim. Dyn. 32, 273–285.

Longinelli, A., Selmo, E., 2003. Isotopic composition of precipitation in Italy: a first overall map. J. Hydrol. 270, 75–88.

López-Tirado, J., Vessella, F., Schirone, B., Hidalgo, P.J., 2018. Trends in evergreen oak suitability from assembled species distribution models: assessing climate change in south-western Europe. N. For. 49, 471–487.

Lubell, D., Mussi, M., Musacchio, A., Agostini, S., Coubray, S., Giraudi, C., 1995. Exploitation of seasonal Resources in the mountains of Abruzzo (Central Italy): Epigravettian to Neolithic. In: Bintz, P., Thévinin, A. (Eds.), L'Europe des derniers chasseurs: Épipaléolithique et Mésolithique. CTHS (5° Congrès UISPP), Paris, pp. 465–472.

Magri, D., Sadori, L., 1999. Late Pleistocene and Holocene pollen stratigraphy at Lago di Vico, central Italy. Veg. Hist. Archaeobotany 8, 247–260.

Mannella, G., 2020. Ricostruzione paleoambientale e paleoclimatica nella regione Mediterranea occidentale attraverso lo studio goechimico e mineralogico della successione sedimentaria del Lago Fucino (Avezzano, Abruzzo). University of Pisa.

Mannella, G., Giaccio, B., Zanchetta, G., Regattieri, E., Leicher, N., Scheidt, S., Grelle, T., Lehne, C., Rolf, C., Wonik, T., Nomade, S., Pereira, A., Niespolo, E., Renne, P., Leng, M., Dean, J., Thomas, C., Ariztegui, D., Gaeta, M., Florindo, F., Paolo Cavinato, G., Provenzale, A., Wagner, B., 2018. Fucino palaeo-lake: towards the palaeoenvironmental history of the last 430 ka. In: *Quaternary: Past, Present, Future - AIQUA Conference*, Florence: Alpine and Mediterranean Quaternary, pp. 137–141.

Mannella, G., Giaccio, B., Zanchetta, G., Regattieri, E., Niespolo, E.M., Pereira, A., Renne, P.R., Nomade, S., Leicher, N., Perchiazzi, N., Wagner, B., 2019. Palaeoenvironmental and palaeohydrological variability of mountain areas in the central Mediterranean region: a 190 ka-long chronicle from the independently dated Fucino palaeolake record (central Italy). Quat. Sci. Rev. 210, 190–210.

Mannella, G., Zanchetta, G., Regattieri, E., Perchiazzi, N., Drysdale, R.N., Giaccio, B., Leng, M.J., Wagner, B., 2020. Effects of organic removal techniques prior to carbonate stable isotope analysis of lacustrine marls: a case study from palaeo-lake Fucino (central Italy). Rapid Commun. Mass Spectrom. 34, 1–8.

Margottini, C., Martini, G., Slejko, D., 1993. Instrumental seismological data since 1900 for northeastern Italy. Earthq. Eng. Struct. Dyn. 22, 1017–1030.

Mariachiara, C., Colasanti, L., Valentina, M., Petitta, M., Aravena, R., 2014. Nitrate contamination of groundwater and surface water (Fucino Plain, Abruzzo): an update on nitrogen cycle and water quality issues. In: Flowpath 2014 - National Meeting on Hydrogeology, pp. 14–15.

Marino, G., Rohling, E.J., Rodríguez-Sanz, L., Grant, K.M., Heslop, D., Roberts, A.P., Stanford, J.D., Yu, J., 2015. Bipolar seesaw control on last interglacial sea level. Nature 522, 197–201.

Martin-Puertas, C., Brauer, A., Wulf, S., Ott, F., Lauterbach, S., Dulski, P., 2014. Annual proxy data from Lago Grande di Monticchio (southern Italy) between 76 and 112 ka: new chronological constraints and insights on abrupt climatic oscillations. Clim. Past 10, 2099–2114.

Martrat, B., Grimalt, J.O., Lopez-Martinez, C., Cacho, I., Sierro, F.J., Flores, J.A., Zahn, R., Canals, M., Curtis, J.H., Hodell, D.A., 2004. 'Abrupt temperature changes in the western mediterranean over the past 250,000 Years', *science*. Am. Assoc. Adv. Sci. 306, 1762–1765.

Masson-Delmotte, V., Buiron, D., Ekaykin, A., Frezzotti, M., Gallée, H., Jouzel, J., Krinner, G., Landais, A., Motoyama, H., Oerter, H., Pol, K., Pollard, D., Ritz, C., Schlosser, E., Sime, L.C., Sodemann, H., Stenni, B., Uemura, R., Vimeux, F., 2011. A comparison of the present and last interglacial periods in six Antarctic ice cores. Clim. Past 7, 397–423.

Masson-Delmotte, V., Schulz, M., Abe-Ouchi, A., Beer, J., Ganopolski, A., Gonzalez Rouco, J.F., Jansen, E., Lambeck, K., Luterbacher, J., Naish, T., Osborn, T., Otto-Bliesner, B., Quinn, T., Ramesh, R., Rojas, M., Shao, X., Timmermann, A., 2013. Information from paleoclimate archives. In: Stocker, T.F., Qin, D., Plattner, G.K., Tignor, M., Allen, S.K., Doschung, J., Nauels, A., Xia, Y., Bex, V., Midgley, P.M. (Eds.), Information from Paleoclimate Archives. in: Climate Change 2013: the Physical Science Basis. Contribution of Working Group I to the Fifth Assessment Report of the Intergovernmental Panel on Climate Change. Cambridge University Press, Cambridge, pp. 383–464.

Mayewski, P.A., Meeker, L.D., Twickler, M.S., Whitlow, S., Yang, Q., Lyons, W.B., Prentice, M., 1997. Major features and forcing of high-latitude northern hemisphere atmospheric circulation using a 110,000-year-long glaciochemical series. J. Geophys. Res.: Ocean 102, 26345–26366.

McManus, J.F., Bond, G.C., Broecker, W.S., Johnsen, S., Labeyrie, L., Higgins, S., 1994. High-resolution climate records from the North Atlantic during the last interglacial. Nature 371, 326–329.

MedECC, 2020. Climate and environmental change in the Mediterranean basin – current situation and risks for the future. *First Mediterranean Assessment Report*, Marseille, France: Union for the Mediterranean, Plan Bleu. UNEP/MAP, p. 632.

Melles, M., Brigham-Grette, J., Minyuk, P.S., Nowaczyk, N.R., Wennrich, V., DeConto, R. M., Anderson, P.M., Andreev, A.A., Coletti, A., Cook, T.L., Haltia-Hovi, E., Kukkonen, M., Lozhkin, A.V., Rosén, P., Tarasov, P., Vogel, H., Wagner, B., 2012. '2.8 million Years of Arctic climate change from lake El'gygytgyn, NE Russia', *science*. Am. Assoc. Adv. Sci. 337, 315–320.

Milner, A.M., Collier, R.E.L., Roucoux, K.H., Müller, U.C., Pross, J., Kalaitzidis, S., Christanis, K., Tzedakis, P.C., 2012. Enhanced seasonality of precipitation in the Mediterranean during the early part of the Last Interglacial. Geology 40, 919–922.

Milner, A.M., Müller, U.C., Roucoux, K.H., Collier, R.E.L., Pross, J., Kalaitzidis, S., Christanis, K., Tzedakis, P.C., 2013. Environmental variability during the Last Interglacial: a new high-resolution pollen record from Tenaghi Philippon, Greece. J. Quat. Sci. 28, 113–117.

Milner, A.M., Roucoux, K.H., Collier, R.E.L., Müller, U.C., Pross, J., Tzedakis, P.C., 2016. Vegetation responses to abrupt climatic changes during the last interglacial complex (marine isotope stage 5) at Tenaghi Philippon, NE Greece. Quat. Sci. Rev. 154, 169–181.

Miola, A., Bondesan, A., Corain, L., Favaretto, S., Mozzi, P., Piovan, S., Sostizzo, I., 2006. Wetlands in the Venetian Po plain (northeastern Italy) during the last glacial maximum: interplay between vegetation, hydrology and sedimentary environment. Quat. Non Pollen Palyn. 141, 53–81.

Mokeddem, Z., McManus, J.F., Oppo, D.W., 2014. Oceanographic Dynamics and the End of the Last Interglacial in the Subpolar North Atlantic, vol. 111. Proceedings of the National Academy of Sciences, pp. 11263–11268.

Monaco, L., Palladino, D.M., Gaeta, M., Marra, F., Sottili, G., Leicher, N., Mannella, G., Nomade, S., Pereira, A., Regattieri, E., Wagner, B., Zanchetta, G., Albert, P.G., Arienzo, I., D'Antonio, M., Petrosino, P., Manning, C.J., Giaccio, B., 2021. Mediterranean tephrostratigraphy and peri-Tyrrhenian explosive activity revaluated in light of the 430-365 ka record from Fucino Basin (central Italy). Earth Sci. Rev. 220.

Monaco, L., Leicher, N., Palladino, D.M., Arienzo, I., Marra, F., Petrelli, M., Nomade, S., Pereira, A., Sottili, G., Conticelli, S., D'Antonio, M., Fabbrizio, A., Jicha, B.R., Mannella, G., Petrosino, P., Regattieri, E., Tzedakis, P.C., Wagner, B., Zanchetta, G., Giaccio, B., 2022a. The Fucino 250–170 ka tephra record: new insights on peri-Tyrrhenian explosive volcanism, central mediterranean tephrochronology, and timing of the MIS 8-6 climate variability. Quat. Sci. Rev. 296, 1–30.

Monaco, L., Palladino, D.M., Albert, P.G., Arienzo, I., Conticelli, S., Di Vito, M., Fabbrizio, A., D'Antonio, M., Isaia, R., Manning, C.J., Nomade, S., Pereira, A., Petrosino, P., Sottili, G., Sulpizio, R., Zanchetta, G., Giaccio, B., 2022b. Linking the Mediterranean MIS 5 tephra markers to Campi Flegrei (southern Italy) 109–92 ka explosive activity and refining the chronology of MIS 5c-d millennial-scale climate variability. Global Planet. Change 211.

Moore, P.D., Webb, J.A., Collinson, M.E., 1991. Pollen Analysis. Blackwell Scientific Publications.

Moss, B., Mckee, D., Atkinson, D., Collings, S.E., Eaton, J.W., Gill, A.B., Harvey, I., Hatton, K., Heyes, T., Wilson, D., 2003. How important is climate? Effects of warming, nutrient addition and fish on phytoplankton in shallow lake microcosms. J. Appl. Ecol. 40, 782–792.

Mottl, O., Grytnes, J.-A., Seddon, A.W.R., Steinbauer, M.J., Bhatta, K.P., Felde, V.A., Flantua, S.G.A., Birks, H.J.B., 2020. R-Ratepol package. Github. Available at: https://github.com/HOPE-UIB-BIO/R-Ratepol-package.

Mottl, O., Grytnes, J.-A., Seddon, A.W.R., Steinbauer, M.J., Bhatta, K.P., Felde, V.A., Flantua, S.G.A., Birks, H.J.B., 2021. Rate-of-change analysis in paleoecology revisited: a new approach. Rev. Palaeobot. Palynol. 293, 1–12.

Natali, S., Baneschi, I., Doveri, M., Giannecchini, R., Selmo, E., Zanchetta, G., 2021. Meteorological and geographical control on stable isotopic signature of precipitation in a western Mediterranean area (Tuscany, Italy): disentangling a complex signal. J. Hydrol. 603, 1–18.

NEEM community members, 2013. Eemian interglacial reconstructed from a Greenland folded ice core. Nature 493, 489–494.
Negrini, R.M., Wigand, P.E., Draucker, S., Gobalet, K., Gardner, J.K., Sutton, M.Q., Yohe, R.M., 2006. The Rambla highstand shoreline and the Holocene lake-level history of Tulare Lake, California, USA. Quat. Sci. Rev. 25, 1599–1618.
NGRIP members, 2004. High-resolution record of Northern Hemisphere climate extending into the last interglacial period. Nature 431, 147–151.
Nicholl, J.A.L., Hodell, D.A., Naafs, B.D.A., Hillaire-Marcel, C., Channell, J.E.T., Romero, O.E., 2012. A Laurentide outburst flooding event during the last interglacial period. Nat. Geosci. 5, 901–904.
Nielsen, H., Sørensen, I., 1992. Taxonomy and stratigraphy of late-glacial Pediastrum taxa from Lysmosen, Denmark — a preliminary study. Rev. Palaeobot. Palynol. 74, 55–75.
Niemeyer, B., Herzschuh, U., Pestryakova, L., 2015. Vegetation and lake changes on the southern Taymyr peninsula, northern Siberia, during the last 300 years inferred from pollen and Pediastrum green algae records. Holocene SAGE Publ. Ltd. 25, 596–606.
Oppo, D.W., Keigwin, L.D., McManus, J.F., Cullen, J.L., 2001. Persistent suborbital climate variability in marine isotope stage 5 and termination II. Paleoceanography 16, 280–292.
Oppo, D.W., McManus, J.F., Cullen, J.L., 2006. Evolution and demise of the last interglacial warmth in the subpolar North Atlantic. Crit. Quat. Stratigr. 25, 3268–3277.
Otto-Bliesner, B.L., Rosenbloom, N., Stone, E.J., McKay, N.P., Lunt, D.J., Brady, E.C., Overpeck, J.T., 2013. How warm was the last interglacial? New model–data comparisons. Phil. Trans. Math. Phys. Eng. Sci. 371, 1–20.
Otto-Bliesner, B.L., Brady, E.C., Zhao, A., Brierley, C.M., Axford, Y., Capron, E., Govin, A., Hoffman, J.S., Isaacs, E., Kageyama, M., Scussolini, P., Tzedakis, P.C., Williams, C.J.R., Wolff, E., Abe-Ouchi, A., Braconnot, P., Ramos Buarque, S., Cao, J., de Vernal, A., Guarino, M.V., Guo, C., LeGrande, A.N., Lohmann, G., Meissner, K.J., Menviel, L., Morozova, P.A., Nisancioglu, K.H., O'ishi, R., Salas y Mélia, D., Shi, X., Sicard, M., Sime, L., Stepanek, C., Tomas, R., Volodin, E., Yeung, N.K.H., Zhang, Q., Zhang, Z., Zheng, W., 2021. Large-scale features of last interglacial climate: results from evaluating the *lig127k* simulations for the coupled model intercomparison project (CMIP6)–Paleoclimate modeling intercomparison project (PMIP4). Clim. Past 17, 63–94.
Pacioni, E., 2008. *Modellazione del flusso e del transporto di pesticidi nel mezzo non saturo in relazione alla vulnerabilità dell'aquifero alluvionale poroso della piana del Fucino*, Dottorato di Ricerca in Scienze della Terra XXI ciclo. Università di Roma Sapienza.
Paerl, H.W., Huisman, J., 2009. Climate change: a catalyst for global expansion of harmful cyanobacterial blooms. Environ. Microbial. Rep. 1, 27–37.
Past Interglacials Working Group of PAGES, 2016. Interglacials of the last 800,000 years. Rev. Geophys. 54, 162–219.
Paterne, M., Guichard, F., Duplessy, J.C., Siani, G., Sulpizio, R., Labeyrie, J., 2008. A 90,000–200,000 yrs marine tephra record of Italian volcanic activity in the Central Mediterranean Sea. J. Volcanol. Geotherm. Res. 177, 187–196.
Pedersen, R.A., Langen, P.L., Vinther, B.M., 2017. The last interglacial climate: comparing direct and indirect impacts of insolation changes. Clim. Dyn. 48, 3391–3407.
Peguero-Pina, J.J., Sancho-Knapik, D., Morales, F., Flexas, J., Gil-Pelegrín, E., 2009. Differential photosynthetic performance and photoprotection mechanisms of three Mediterranean evergreen oaks under severe drought stress. Funct. Plant Biol. 36, 453–462.
Petitta, M., Fracchiolla, D., Aravena, R., Barbieri, M., 2009. Application of isotopic and geochemical tools for the evaluation of nitrogen cycling in an agricultural basin, the Fucino Plain, Central Italy. J. Hydrol. 372, 124–135.
Petroselli, A., Vessella, F., Cavagnuolo, L., Piovesan, G., Schirone, B., 2013. Ecological behavior of Quercus suber and Quercus ilex inferred by topographic wetness index (TWI). Trees (Berl.) 27, 1201–1215.
Petrosino, P., Morabito, S., Jicha, B.R., Milia, A., Sprovieri, M., Tamburrino, S., 2016. Multidisciplinary tephrochronological correlation of marker events in the eastern Tyrrhenian Sea between 48 and 105ka. J. Volcanol. Geoth. Res. 315, 79–99.
Phillips, L., 1974. Vegetational History of the Ipswichian/Eemian Interglacial in Britain and Continental Europe, vol. 73. John Wiley & Sons, Ltd, New Phytologist, pp. 589–604.
Piccini, L., Zanchetta, G., Drysdale, R., Hellstrom, J., Isola, I., Fallick, A.E., Leone, G., Doveri, M., Mussi, M., Mantelli, F., Molli, G., Lotti, L., Roncioni, A., Regattieri, E., Mecceri, M., Vaselli, L., 2008. The environmental features of the Monte Corchia cave system (Apuan Alps, central Italy) and their effects on speleothem growth. Int. J. Speleol. 37, 153–172.
Pickarski, N., Kwiecien, O., Djamali, M., Litt, T., 2015. Vegetation and environmental changes during the last interglacial in eastern Anatolia (Turkey): a new high-resolution pollen record from Lake Van. Palaeogeogr. Palaeoclimatol. Palaeoecol. 435, 145–158.
Pignatti, S., 1982. Flora d'Italia, Italy: Edagricole.
Pini, R., Ravazzi, C., Reimer, P.J., 2010. The vegetation and climate history of the last glacial cycle in a new pollen record from Lake Fimon (southern Alpine foreland, N-Italy). Quat. Sci. Rev. 29, 3115–3137.
Pons, A., Reille, M., 1988. The Holocene- and upper Pleistocene pollen record from Padul (Granada, Spain): a new study. Palaeogeogr. Palaeoclimatol. Palaeoecol. 66, 243–263.
Prentice, C., Guiot, J., Huntley, B., Jolly, D., Cheddadi, R., 1996. Reconstructing biomes from palaeoecological data: a general method and its application to European pollen data at 0 and 6 ka. Clim. Dyn. 12, 185–194.
R Core Team, 2022. R: A Language and Environment for Statistical Computing. R Foundation for Statistical Computing, Vienna, Austria.
Ralska-Jasiewiczowa, M., Goslar, T., Różański, K., Wacnik, A., Czernik, J., Chróst, L., 2003. Very fast environmental changes at the Pleistocene/Holocene boundary, recorded in laminated sediments of Lake Gościąż, Poland. Palaeogeogr. Palaeoclimatol. Palaeoecol. 193, 225–247.
Rasconi, S., Gall, A., Winter, K., Kainz, M.J., 2015. 'Increasing water temperature triggers dominance of small freshwater Plankton', *PLOS ONE*. Publ. Library Sci. 10, 1–17.
Ravazzi, C., 2002. Late Quaternary history of spruce in southern Europe. Rev. Palaeobot. Palynol. 120, 131–177.
Reale, M., Lionello, P., 2013. Synoptic climatology of winter intense precipitation events along the Mediterranean coasts. Nat. Hazards Earth Syst. Sci. 13, 1707–1722.
Regattieri, E., Giaccio, B., Zanchetta, G., Drysdale, R.N., Galli, P., Nomade, S., Peronace, E., Wulf, S., 2015. Hydrological variability over the Apennines during the Early Last Glacial precession minimum, as revealed by a stable isotope record from Sulmona basin, Central Italy. J. Quat. Sci. John Wiley Son Ltd 30, 19–31.
Regattieri, E., Zanchetta, G., Drysdale, R.N., Isola, I., Hellstrom, J.C., Roncioni, A., 2014. A continuous stable isotope record from the penultimate glacial maximum to the Last Interglacial (159–121ka) from Tana Che Urla Cave (Apuan Alps, central Italy). Quat. Res. 82, 450–461.
Reille, M., 1999. Pollen et Spores d'Europe et d'Afrique du nord. Laboratoire de Botanique Historique et Palynologie, Marseille, France.
Reynolds, C.S., 1984. Phytoplankton periodicity: the interactions of form, function and environmental variability. Freshwater Biol. 14, 111–142.
Roberts, N., Jones, M.D., Benkaddour, A., Eastwood, W.J., Filippi, M.L., Frogley, M.R., Lamb, H.F., Leng, M.J., Reed, J.M., Stein, M., Stevens, L., Valero-Garcés, B., Zanchetta, G., 2008. Stable isotope records of Late Quaternary climate and hydrology from Mediterranean lakes: the ISOMED synthesis. Quat. Sci. Rev. 27, 2426–2441.
Rohling, E., Mayewski, P., Abu-Zied, R., Casford, J., Hayes, A., 2002. Holocene atmosphere-ocean interactions: records from Greenland and the Aegean Sea. Clim. Dyn. 18, 587–593.
Rohling, E.J., Grant, K., Hemleben, Ch, Siddall, M., Hoogakker, B.A.A., Bolshaw, M., Kucera, M., 2007. High rates of sea-level rise during the last interglacial period. Nat. Geosci. 1, 38–42.
Roucoux, K.H., Tzedakis, P.C., Frogley, M.R., Lawson, I.T., Preece, R.C., 2008. Vegetation history of the marine isotope stage 7 interglacial complex at Ioannina, NW Greece. Quat. Sci. Rev. 27, 1378–1395.
Roucoux, K.H., Tzedakis, P.C., Lawson, I.T., Margari, V., 2011. Vegetation history of the penultimate glacial period (Marine isotope stage 6) at Ioannina, north-west Greece. J. Quat. Sci. John Wiley Son Ltd 26, 616–626.
Rull, V., López-Sáez, J.A., Vegas-Vilarrúbia, T., 2008. Contribution of non-pollen palynomorphs to the paleolimnological study of a high-altitude Andean lake (Laguna Verde Alta, Venezuela). J. Paleolimnol. 40, 399–411.
Sadori, L., Koutsodendris, A., Panagiotopoulos, K., Masi, A., Bertini, A., Combourieu-Nebout, N., Francke, A., Kouli, K., Joannin, S., Mercuri, A.M., Peyron, O., Torri, P., Wagner, B., Zanchetta, G., Sinopoli, G., Donders, T.H., 2016. Pollen-based paleoenvironmental and paleoclimatic change at Lake Ohrid (south-eastern Europe) during the past 500 ka. Biogeosciences 13, 1423–1437.
Sánchez Goñi, M.F., Loutre, M.F., Crucifix, M., Peyron, O., Santos, L., Duprat, J., Malaizé, B., Turon, J.-L., Peypouquet, J.-P., 2005. Increasing vegetation and climate gradient in Western Europe over the Last Glacial Inception (122–110 ka): data-model comparison. Earth Planet Sci. Lett. 231, 111–130.
Scheffer, M., Carpenter, S.R., 2003. Catastrophic regime shifts in ecosystems: linking theory to observation. Trends Ecol. Evol. 18, 648–656.
Scheffer, M., Carpenter, S., Foley, J.A., Folke, C., Walker, B., 2001. Catastrophic shifts in ecosystems. Nature 413, 591–596.
Seddon, A.W., Macias-Fauria, M., Willis, K.J., 2015. Climate and abrupt vegetation change in Northern Europe since the last deglaciation. Holocene SAGE Publ. Ltd. 25, 25–36.
Seppä, H., 2013. Pollen analysis, principles. In: Elias, S.A., Mock, C.J. (Eds.), Encyclopedia of Quaternary Science, second ed. Elsevier, Amsterdam, pp. 794–804.
Shackleton, S., Baggenstos, D., Menking, J.A., Dyonisius, M.N., Bereiter, B., Bauska, T.K., Rhodes, R.H., Brook, E.J., Petrenko, V.V., McConnell, J.R., Kellerhals, T., Häberli, M., Schmitt, J., Fischer, H., Severinghaus, J.P., 2020. Global ocean heat content in the Last Interglacial. Nat. Geosci. 13, 77–81.
Sinopoli, G., Masi, A., Regattieri, E., Wagner, B., Francke, A., Peyron, O., Sadori, L., 2018. Palynology of the last interglacial complex at Lake Ohrid: palaeoenvironmental and palaeoclimatic inferences. Quat. Sci. Rev. 180, 177–192.
Šmilauer, P., Lepš, J., 2014. Multivariate Analysis of Ecological Data Using CANOCO 5, second ed. Cambridge University Press, Cambridge.
Spell, T.L., Smith, E.I., Sanford, A., Zanetti, K.A., 2001. Systematics of xenocrystic contamination: preservation of discrete feldspar populations at McCullough Pass Caldera revealed by 40Ar/39Ar dating. Earth Planet Sci. Lett. 190, 153–165.
Stockmarr, J., 1971. Tablets with spores used in absolute pollen analysis. Pollen Spores 13, 615–621.
Swain, A.M., 1973. A history of fire and vegetation in northeastern Minnesota as recorded in lake sediments. Ecol. Role Fire Nat.Conf. Forest West. North. Am. 3, 383–396.
Ter Braak, C.J.F., Šmilauer, P., 2018. Canoco reference manual and user's guide: software for ordination (version 5.10). Biometris Wagening. Univ. Res.
Terradas, J., 1999. Ecology of mediterranean evergreen oak forests. In: Rodà, F., Retana, J., Gracia, C., Bellot, J. (Eds.), Ecological Studies. Springer, Berlin, Heidelberg, pp. 3–14.
Tinner, W., Hu, F.S., 2003. Size parameters, size-class distribution and area-number relationship of microscopic charcoal: relevance for fire reconstruction. Holocene 13, 499–505.

Tomlinson, E.L., Albert, P.G., Wulf, S., Brown, R.J., Smith, V.C., Keller, J., Orsi, G., Bourne, A.J., Menzies, M.A., 2014. Age and geochemistry of tephra layers from Ischia, Italy: constraints from proximal-distal correlations with Lago Grande di Monticchio. J. Volcanol. Geoth. Res. 287, 22–39.
Turner, C., 1975. The correlation and duration of middle Pleistocene interglacial periods in northwest Europe. In: Butzer, K.W., Isaac, G.L. (Eds.), After the Australopithecines: Stratigraphy, Ecology and Culture Change in the Middle Pleistocene. De Gruyter Mouton, Berlin, pp. 259–308.
Turner, R., Roberts, N., Jones, M.D., 2008. Climatic pacing of Mediterranean fire histories from lake sedimentary microcharcoal. Global Planet. Change 63, 317–324.
Tzedakis, P.C., 1993. Long-term tree populations in northwest Greece through multiple Quaternary climatic cycles. Nature 364, 437–440.
Tzedakis, P.C., 1994. 'Vegetation change through glacial-interglacial cycles: a long pollen sequence perspective', *philosophical transactions: biological sciences*. Royal Soc. 345, 403–432.
Tzedakis, P.C., 2007. Seven ambiguities in the Mediterranean palaeoenvironmental narrative. Quat. Sci. Rev. 26, 2042–2066.
Tzedakis, P.C., 2009. Museums and cradles of Mediterranean biodiversity. J Biogeogr. 36, 1033–1034.
Tzedakis, P.C., Andrieu, V., de Beaulieu, J.-L., Crowhurst, S., Follieri, M., Hooghiemstra, H., Magri, D., Reille, M., Sadori, L., Shackleton, N.J., Wijmstra, T.A., 1997. Comparison of terrestrial and marine records of changing climate of the last 500,000 years. Earth Planet Sci. Lett. 150, 171–176.
Tzedakis, P.C., Frogley, M.R., Heaton, T.H.E., 2002. Duration of last interglacial conditions in Northwestern Greece. Quat. Res. 58, 53–55.
Tzedakis, P.C., Frogley, M.R., Heaton, T.H.E., 2003. Last Interglacial conditions in southern Europe: evidence from Ioannina, northwest Greece. Global Planet. Change 36, 157–170.
Tzedakis, P.C., Hooghiemstra, H., Pälike, H., 2006. The last 1.35 million years at Tenaghi Philippon: revised chronostratigraphy and long-term vegetation trends. Crit. Quat. Stratigr. 25, 3416–3430.
Tzedakis, P.C., Drysdale, R.N., Margari, V., Skinner, L.C., Menviel, L., Rhodes, R.H., Taschetto, A.S., Hodell, D.A., Crowhurst, S.J., Hellstrom, J.C., Fallick, A.E., Grimalt, J.O., McManus, J.F., Martrat, B., Mokeddem, Z., Parrenin, F., Regattieri, E., Roe, K., Zanchetta, G., 2018. Enhanced climate instability in the North Atlantic and southern Europe during the last interglacial. Nat. Commun. 9, 1–14.
Ulbrich, U., Lionello, P., Belusic, D., Jacobeit, J., Knippertz, P., Kuglitsch, F.G., Leckebusch, G.C., Luterbacher, J., Maugeri, M., Maheras, P., Nissen, K., Pavan, V., Pinto, J., Saaroni, H., Seubert, S., Toreti, A., Xoplaki, E., Ziv, B., 2012. Climate of the mediterranean: synoptic patterns, temperature, precipitation, winds, and their extremes. In: Lionello, P. (Ed.), Climate of the Mediterranean Region - from the Past to the Future. Elsevier, pp. 301–346.
Van Geel, B., 2001. Non-pollen palynomorphs. In: Smol, J., Birks, H.J.B., Last, W.M., Bradley, R.S., Alverson, K. (Eds.), Traking Environmental Change Using Lake Sediments. Vol 3: Terrestrial, Algal, and Silicaceous Inidcators. Springer, Dordrecht, pp. 99–119.
Van Geel, B., Mur, L.R., Ralska-Jasiewiczowa, M., Goslar, T., 1994. Fossil akinetes of aphanizomenon and Anabaena as indicators for medieval phosphate-eutrophication of Lake gosciaz (Central Poland). Rev. Palaeobot. Palynol. 83, 97–105.
Vannière, B., Power, M.J., Roberts, N., Tinner, W., Carrión, J., Magny, M., Bartlein, P., Colombaroli, D., Daniau, A.L., Finsinger, W., Gil-Romera, G., Kaltenrieder, P., Pini, R., Sadori, L., Turner, R., Valsecchi, V., Vescovi, E., 2011. Circum-Mediterranean fire activity and climate changes during the mid-Holocene environmental transition (8500-2500 cal. BP). Holocene SAGE Publ. Ltd. 21, 53–73.
Visbeck, M.H., Hurrell, J.W., Polvani, L., Cullen, H.M., 2001. The North Atlantic oscillation: past, present, and future. Proc. Nat. Acad. Sci. 98, 12876–12877.
Watts, W.A., 1985. A long pollen record from Laghi di Monticchio, southern Italy: a preiminary account. J. Geol. Soc. 142, 491–499.
Watts, W.A., Allen, J.R.M., Huntley, B., 1996. Vegetation history and palaeoclimate of the last glacial period at Lago Grande di Monticchio, Southern Italy. Quat. Sci. Rev. 15, 133–153.
Whitney, B.S., Mayle, F.E., 2012. Pediastrum species as potential indicators of lake-level change in tropical South America. J. Paleolimnol. 47, 601–615.
Wijmstra, T.A., 1969. Palynology of the first 30 meters of a 120 m deep section in northern Greece. Acta Bot. Neerl. 18, 511–527.
Wijmstra, T.A., Smit, A., 1976. Palynology of the middle part (30-78 metres) of the 120 m deep section in northern Greece (Macedonia). Acta Bot. Neerl. 25, 297–312.
Wulf, S., Kraml, M., Brauer, A., Keller, J., Negendank, J.F.W., 2004. Tephrochronology of the 100ka lacustrine sediment record of Lago Grande di Monticchio (southern Italy). Quat. Int. 122, 7–30.
Wulf, S., Keller, J., Paterne, M., Mingram, J., Lauterbach, S., Opitz, S., Sottili, G., Giaccio, B., Albert, P.G., Satow, C., Tomlinson, E.L., Viccaro, M., Brauer, A., 2012. The 100–133 ka record of Italian explosive volcanism and revised tephrochronology of Lago Grande di Monticchio. Quat. Sci. Rev. 58, 104–123.
Wulf, S., Hardiman, M.J., Staff, R.A., Koutsodendris, A., Appelt, O., Blockley, S.P.E., Lowe, J.J., Manning, C.J., Ottolini, L., Schmitt, A.K., Smith, V.C., Tomlinson, E.L., Vakhrameeva, P., Knipping, M., Kotthoff, U., Milner, A.M., Müller, U.C., Christanis, K., Kalaitzidis, S., Tzedakis, P.C., Schmiedl, G., Pross, J., 2018. The marine isotope stage 1–5 cryptotephra record of Tenaghi Philippon, Greece: towards a detailed tephrostratigraphic framework for the Eastern Mediterranean region. Quat. Sci. Rev. 186, 236–262.
Xoplaki, E., González-Rouco, J.F., Luterbacher, J., Wanner, H., 2003. Mediterranean summer air temperature variability and its connection to the large-scale atmospheric circulation and SSTs. Clim. Dyn. 20, 723–739.
Zanchetta, G., Bonadonna, F.P., Leone, G., 1999. A 37-Meter Record of Paleoclimatological Events from Stable Isotope Data on Continental Molluscs in Valle di Castiglione, Near Rome, Italy. Quat. Res. 52, 293–299.
Zanchetta, G., Drysdale, R.N., Hellstrom, J.C., Fallick, A.E., Isola, I., Gagan, M.K., Pareschi, M.T., 2007. Enhanced rainfall in the Western Mediterranean during deposition of sapropel S1: stalagmite evidence from Corchia cave (Central Italy). Quat. Sci. Rev. 26, 279–286.
Zanchetta, G., Bini, M., Bloomfield, K., Izdebski, A., Vivoli, N., Regattieri, E., Isola, I., Drysdale, R.N., Bajo, P., Hellstrom, J.C., Wiśniewski, R., Fallick, A.E., Natali, S., Luppichini, M., 2021. Beyond one-way determinism: San Frediano's miracle and climate change in Central and Northern Italy in late antiquity. Clim. Change 165, 1–21.
Zanchetta, G., Baneschi, I., Magny, M., Sadori, L., Termine, R., Bini, M., Vannière, B., Desmet, M., Natali, S., Luppichini, M., Pasquetti, F., 2022. Insight into summer drought in southern Italy: palaeohydrological evolution of Lake Pergusa (Sicily) in the last 6700 years. J. Quat. Sci. 37, 1280–1293.
Zanchetta, G., Regattieri, E., Giaccio, B., Wagner, B., Sulpizio, R., Francke, A., Vogel, H., Sadori, L., Masi, A., Sinopoli, G., Lacey, J.H., Leng, M.J., Leicher, N., 2016. Aligning and synchronization of MIS5 proxy records from Lake Ohrid (FYROM) with independently dated Mediterranean archives: implications for DEEP core chronology. Biogeosciences 13, 2757–2768.
Zielhofer, C., Fletcher, W.J., Mischke, S., De Batist, M., Campbell, J.F.E., Joannin, S., Tjallingii, R., El Hamouti, N., Junginger, A., Stele, A., Bussmann, J., Schneider, B., Lauer, T., Spitzer, K., Strupler, M., Brachert, T., Mikdad, A., 2017. Atlantic forcing of Western Mediterranean winter rain minima during the last 12,000 years. Quat. Sci. Rev. 157, 29–51.